ROYAL SOCIETY
OF CHEMISTRY

Check for updates

Plasmonic and metamaterial biosensors: a game-changer for virus detection

Junfei Wang, [iD] [a] Zhenyu Xu [iD] [a] and Domna G. Kotsifaki [iD] *[ab]

One of the most important processes in the fight against current and future pandemics is the rapid diagnosis and initiation of treatment of viruses in humans. Currently available viral diagnostic methods detect only known pathogens, which comprise a small number of virus strains. In addition, identifying viral genomes is challenging due to low viral abundance and possible contamination by host nucleic acids. To ensure the distinction between the infected and non-infected people and predict the outbreak of disease, alternative approaches should be considered. In the ongoing hunt for new developing tests and diagnostic kits with high selectivity and sensitivity, plasmonic platforms, which control light in subwavelength volumes, have opened up exciting prospects for biosensing applications. They can identify particular viruses in a cost-effective, sensitive, label-free, rapid, and reproducible way due to their tunable plasmonic properties. In particular, plasmonic-assisted virus detection platforms can be achieved by various approaches, including propagating surface and localized plasmon resonances, as well as surface-enhanced Raman spectroscopy. In this review, we discuss both the fundamental principles governing a plasmonic biosensor and prospects for achieving improved sensor performance. We highlight several nanostructure schemes to combat virus-related diseases. We also examine the technological limitations and challenges of plasmonic-based biosensing, such as reducing the overall cost and handling of complex biological samples. Finally, we provide a future perspective for opportunities to improve plasmonic-based approaches to increase their impact on global health issues.

1 Introduction

At the dawn of the twenty-first century, humanity faces multiple health challenges with substantial global economic and social impacts.[1–6] The monitoring and early detection of biological entities necessitate platforms that are able to analyze extremely low concentrations of analytes in real samples near the point of care (PoC) and sometimes at the place of patient care. The early detection and timely treatment of diseases can improve cure rates and reduce treatment costs. Commonly used analytical methods[7–9] rely upon culture-based methods, serological tests, or nucleic acid-based amplification techniques such as polymerase chain reaction (PCR), gene sequencing, virus isolation, hemagglutination assay, and enzyme-linked immunosorbent assay (ELISA). In spite of their inherent advantages, these techniques are time-consuming and involve sophisticated instrumentation that requires skilled operators. In addition, time-consuming predeveloped protocols are typically limited

to specific strains or types of viruses and may have high false-negative rates, which limit their effectiveness to lower the risk of new infections.[10] Viruses are structures of several sizes (from 20 to 900 nm) and morphological shapes, composed of genetic material covered in proteins, glycoproteins, or lipids.[11] Approximately one-third of all infectious disease-related deaths are caused by viral infections.[12] One fundamental issue in considering viral diagnostics sensitivity is the uncertainty about the range of viral loads that constitute a transmission risk.[13] Those infected with SARS-CoV-2, for example, are most infectious around the time of system onset when viral loads in the upper respiratory tract are highest. Similar to pre-symptomatic individuals, asymptotic individuals contribute to viral spread as well.[13] Hence, it is crucial to diagnose viruses during their incubation period in order to maximize healing rates and reduce the risk of pandemics.[12] It is equally important to detect viruses in order to monitor the environment because they can also infect plants and animals.[14] Although PCR can provide accurate and sensitive viral diagnostics by amplification of specific DNA/RNA sequences, it is more expensive than plasmon-based methods.[7–9] Consequently, the need for new diagnostic approaches that are fast and cost-effective has brought into focus the development of real-time PoC testing devices,[15] based on plasmonic nanostructures

[a] *Photonics Lab, Division of Natural and Applied Sciences, Duke Kunshan University, Kunshan, 215316, Jiangsu Province, China.*
E-mail: domna.kotsifaki@dukekunshan.edu.cn, dk310@duke.edu
[b] *Data Science Research Center, Duke Kunshan University, Kunshan, 215316, Jiangsu Province, China*

that offer new sensing capabilities for rapid diagnosis of virus particles and could be a game changer for disease management.

With the growing need for new PoC diagnostic platforms, the World Health Organization has created the ASSURED (affordable, sensitive, specific, user-friendly, rapid and robust, equipment-free, and deliverable to end users) framework, outlining directions and guidelines for their development.[16] Current PoC tests, such as paper-based devices,[17] succeed in providing rapid, cost-effective, and facile results but are held back by inadequate sensitivity, selectivity, and overall reliability, highlighting the challenges faced by PoC diagnostics.[18] Early diagnosis is essential for a wide range of conditions, including infectious diseases, auto-immune disorders, and inflammatory diseases, for which timing is important to maximize the efficacy of therapy. In addition, continuous monitoring of viral biomarkers or therapeutic drug levels at the bedside can provide valuable feedback to physicians and allow them to tailor the treatment options for individual patients.[19–21] In this aspect, nanostructure-based PoC approaches that can rapidly provide the molecular profile of a patient could become instrumental in paving the way towards precision diagnosis.[22,23]

Plasmonic-based biosensing (Fig. 1) has embraced the challenge of offering on-site strategies to complement traditional diagnostic methods and has attracted significant attention owing to its versatility and ability to achieve label-free monitoring with low response times.[5,22,27–33] These characteristics, achieved by exploiting the properties of nanomaterials,[34–39] have allowed for the design of ultrasensitive nanobiosensors, which could be implemented in diagnostic tools to alleviate the burden of infectious diseases in the developing world. By patterning metal films into nanostructures even tighter electromagnetic field confinement is possible, allowing for the detection of single virus particles.[40] Therefore, plasmonic-based biosensing utilizes the interaction of electromagnetic fields to detect virus particles, antigens, or nucleic acids from clinical specimens (such as blood, serum, saliva, *etc.*) with high selectivity and sensitivity. Furthermore, this method offers the advantages of easy operation, minimal sample pretreatment, and simple cost-effective instrumentation.[41] Likewise, as light sources, detectors, and optical components are abundant in the visible-to-near infrared electromagnetic spectrum range, the design of plasmonic biosensors in this
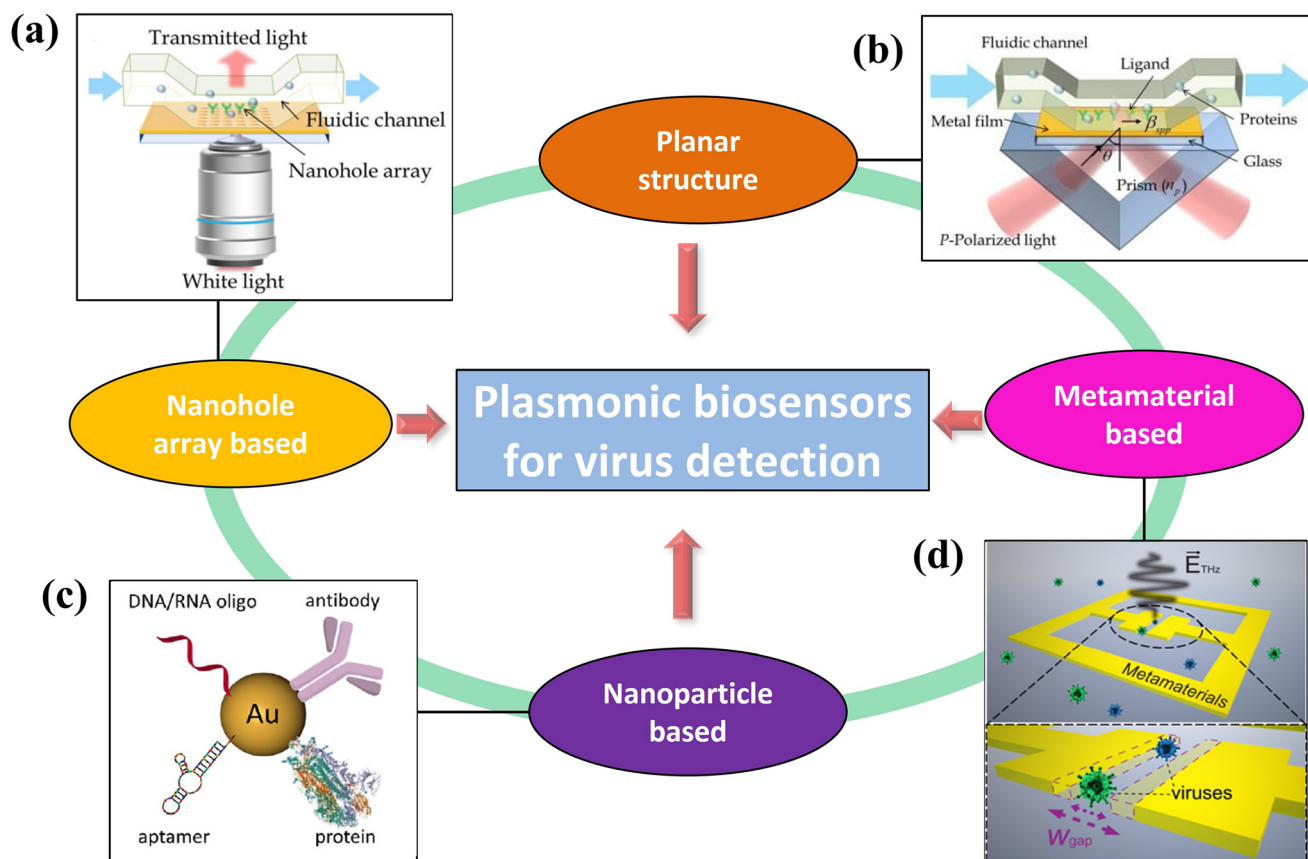

Fig. 1 Schematic illustration of various plasmonic-based virus sensing platforms. (a) An array of nanoholes can increase the binding potential for flowing virus antigens and enhance the sensitivity through the extraordinary transmission effect (reproduced with permission from ref. 24). (b) Planar structure in which surface plasmon is generated in between a dielectric and a metal (reproduced with permission from ref. 24). (c) Localized surface plasmon around nanoparticles can increase sensitivity (reproduced with permission from ref. 25). (d) Metamaterials can efficiently enhance the electromagnetic fields of light, leading to ultrasensitive biosensing (reproduced with permission from ref. 26).

range is particularly advantageous.[24] Such biosensors require structural dimensions on the few-nanometer scale and can be fabricated using nanolithography techniques.[18,24,41,42] In addition, plasmonic biosensors enable direct detection of analytes from heterogeneous biological media without the need for exogenous labels.[43,44] This is a key factor in plasmonic-based biosensor design since it facilitates bio-assay procedures by eliminating tedious washing, amplifying, and labeling steps.[1,10,45] For the abovementioned reasons, plasmonic-based biosensors are seen as promising candidates for the essential elements of future biosensor PoC platforms.

In this tutorial review, we present the advances in plasmonic-based biosensing for virus detection and highlight the scope of future work in this research field. We address the fundamental physical principles of plasmonic effects and biosensing strategies. The integration of metallic nanostructures into commercial microfluidic platforms for future devices that can alert the public to biological threats is also discussed. Because of the ongoing coronavirus disease 2019 (COVID-19) pandemic, slight emphasis is given to coronavirus detection techniques. Finally, we discuss the challenges that need to be overcome for the future development of plasmonic-based biosensors and note how such biosensors are already impacting the diagnosis of infectious diseases in the developing world. We believe that this comprehensive review will be a useful resource for researchers, physicians, and students interested in constructing ultra-dense and high-throughput clinical screening plasmonic devices.

2 Physical considerations

2.1 A brief historical introduction

The interaction of light with plasmonic nanostructures has long been a subject of interest in the classical and quantum worlds.[46] A key feature of plasmon resonances is that they are excited by electromagnetic waves, either evanescent or localized.[46] Their first observation dates back to Wood,[47] who reported anomalous reflective patterns when polarized light was shone on a metalized diffraction grating. A few years later, Rayleigh[48] provided a phenomenological explanation for these patterns, but the underlying physical mechanism remained a mystery. In 1957, significant advances in our understanding of surface plasmon resonance (SPR) were made when Ritchie[49] confirmed the presence of metal surface plasma excitations, while Powell et al. determined that the excitation of surface plasmons involved electrons at metal interfaces.[50] In 1968, Otto used an attenuated total reflection prism-coupled method to enable the coupling of an electromagnetic field with surface plasmon waves.[51] Similarly, Kretschmann and Raether reported the excitation of SPR by utilizing a 10–100 nm thin gold film on the surface of a prism.[52] The potential exploitation of SPR for biosensing first appeared in 1974 with observations made by Fleischmann and

colleagues,[54] who noted an enhancement of Raman scattering near a roughened metal surface; this enhancement was later found to be associated with an electromagnetic effect.[55] Ten years later, Liedberg et al. observed refractive index (RI) changes on the surface of a metallic film after the absorption of biomolecules.[56] Since then, the label-free nature of SPR biosensing has become an important tool in biophysics, molecular biology, and pharmaceutical research.[41,42,57–59] Today, several companies, such as Biocore, PhotonicSys, and Plasmetric, manufacture devices used to evaluate the performance of biosensor chips for PoC applications.

2.2 Fundamental mechanism of plasmon resonance biosensors

2.2.1 Surface plasmon resonance (SPR) mechanism.
Surface plasmon polaritons require a material with free electrons and low optical losses at the optical regime of the electromagnetic wave, i.e., materials that possess a negative real and small positive imaginary dielectric constant.[60–62] Among the materials that exhibit plasmonic properties, conductive noble metals, such as gold and silver, are often used to excite plasmon resonances because of their tunable plasmonic properties in the visible and near-infrared range of the electromagnetic spectrum.[63]

A simple technique of generating surface plasmons from a metal–dielectric interface is the Kretschmann configuration (Fig. 2(a)). The underlying physics of SPR sensors based on an evanescent field has been reviewed extensively in the literature.[44,64,65] Briefly, when light, which implies an electromagnetic wave, strikes the metal, the electric field of the light interacts with conducting electrons. The coupling of the incident electromagnetic wave to the collective oscillations of the conduction electrons forms an evanescent wave, which is known as SPR. To achieve this, the momentum of incident photons should match the momentum of the conduction band of electrons. This momentum matching condition depends on the refractive index (RI) of the dielectric medium at the surface of the metal layer and is given by the following expression:[64]

$$k_{SP} = \frac{2\pi}{\lambda n} \sqrt{\frac{\varepsilon_m \varepsilon_d}{\varepsilon_m + \varepsilon_d}} = \frac{2\pi}{\lambda} n_p \sin\theta \tag{1}$$

where k_{SP} is the surface plasmon wavevector, λ is the wavelength of the incident light, ε_m is the dielectric constant of the metallic film (a function of λ), ε_d (a function of the refractive index of the medium) is the dielectric constant of the surrounding medium, n_p is the refractive index of the coupling prism, and θ is the incident angle of the light. When ε_m and ε_d have equal magnitude and opposite sign, the wavevector, k_{SP}, is at maximum, which results in plasmon resonance conditions. At this matching condition, the reflected light has minimum intensity and θ is called the SPR angle. In particular, the evanescent field is highly sensitive to the RI of the analyte medium causing
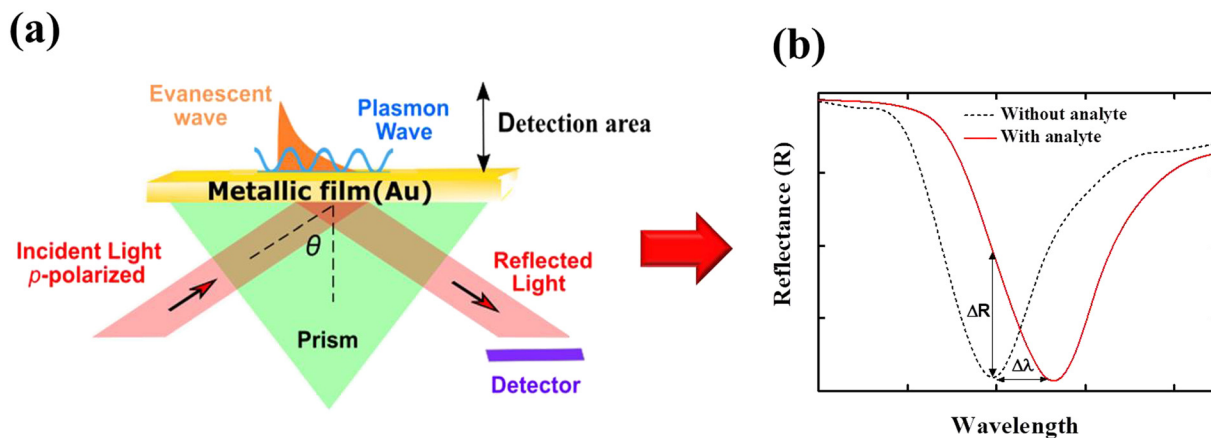
(a)

(b)

Fig. 2 (a) Schematic illustration of the Kretschmann configuration.[53] The surface plasmon polariton can be excited when momentum mismatching is satisfied. The surface plasmon decays exponentially from the surface and propagates to a distance of a few tens of microns. (b) Typical sensor readouts: spectrum of reflected light before and after the binding of the analyte, which leads to refractive index changes. The momentum mismatching condition exists at certain incident angles θ. $\Delta\lambda$ is the resonance shift and ΔR indicates the intensity changes due to analyte binding.

plasmonic property changes (Fig. 2(b)). Therefore, measuring the changes in this resonance condition (for example, angle, wavelength, intensity, or phase), the biomolecular interactions that occur at the biosensor surface can be monitored in real-time.[66]

2.2.2 Localized surface plasmon resonance (LSPR) mechanism. LSPR is another mechanism that has potential applications in high-sensitivity plasmonic biosensing.[38,63,67] Unlike in SPR, the electromagnetic field in LSPR does not propagate but is instead localized around subwavelength nanoparticles or nanostructures bound to the metal.[24,67] The practical application of LSPR can be seen in artifacts dating back to the fourth century, with the Lycurgus cup, an ancient Roman cage cup (currently on display in the British Museum[68]), being one of the best early examples of LSPR. The vessel is made of glass containing silver nanoparticles, leading to a green appearance when viewed with reflected light but a red appearance when viewed with transmitted light (from inside the cup). Specifically, the conduction electrons in the metallic nanoparticles undergo collective harmonic oscillations when under an applied electromagnetic field, resulting in a dipolar response.[43] For a metallic nanoparticle with radius R and dielectric constant ε_m, in a medium with a dielectric constant of ε_d, the exact conditions for LSPR can be solved by applying the Mie theory:[43]

$$\sigma_{ext} = 12\left(\frac{\omega}{c}\right)\pi\varepsilon_d^{3/2}R^3\frac{Im(\varepsilon_m)}{\left[Re(\varepsilon_m) + 2\varepsilon_d\right]^2 + \left[Im(\varepsilon_m)\right]^2} \quad (2)$$

where ω is the angular frequency, and Im and Re are the imaginary and real parts of dielectric constants, respectively. Eqn (2) shows that when the electrons in the metallic nanoparticle oscillate and the real part of the dielectric function is negative, the denominator will vanish, which leads to a strong resonance condition that will shift with local changes in the dielectric environment.[65] In addition,

coherent oscillations of the electrons at resonance make the absorption and scattering cross-sections several orders of magnitude larger than the actual size of the nanoparticles.[65] Eqn (2) is modified with the geometrical form factor, while for any arbitrary shape, more rigorous calculations are needed.[38] Moreover, the performance of LSPR biosensors depends on the resonance properties of the nanostructures, which can be engineered by optimizing the design parameters. For instance, nanorods with a high aspect ratio are more sensitive to RI changes,[63] while larger metallic nanoparticles have smaller repulsion of electrons at opposite surfaces, resulting in plasmon resonance that is more red-shifted; this is suitable for making LSPR-biosensors that can detect and quantify biorecognition events.[69] Additionally, the incident electromagnetic light can be directly coupled to the plasmon field without any coupling configuration, such as prisms or gratings, which improves the complexity of the sensing system. Furthermore, LSPR-based biosensor nanostructures can be fabricated by nanolithography techniques using not only nanoparticles but also chip-based substrates that are miniaturized with high sensitivity and repeatability. This can provide the benefit of being able to integrate the biosensor with other sensing components, such as microfluidics.[70–72]

For the detection mechanisms in both SPR and LSPR, the sensitivity to changes within their associated plasmon decays with length.[65] LSPR changes can be detected within tens of nanometers in the visible range, whereas SPR changes, which occur along the propagation surface, can be detected within a few hundred nanometers.[67] In biosensing, LSPRs are usually utilized through surface-enhanced techniques such as surface-enhanced Raman scattering spectroscopy[73] (SERS), surface-enhanced infrared absorption spectroscopy,[74] surface-enhanced fluorescence,[75] and through resonance shifts induced by nearby analytes.[76]

2.3 Plasmonic metamaterials

Plasmonic metamaterials have been utilized to further control collective plasmonic modes and electromagnetic field enhancement.[77–80] The concept of these materials was first introduced in 1968 by Veselago, who observed the unusual behavior of light refracted by a left-handed material.[81] A few years later, Pendry et al. noted that microstructures, fabricated from nonmagnetic conducting sheets smaller than the excitation wavelength, could be tuned to show varying magnetic permeability, including imaginary components.[82] Based on these observations,[81,82] a practical way to manufacture a left-handed material that does not follow the conventional right-hand was determined. In 2000, Smith et al. demonstrated the first left-handed metamaterial, which simultaneously exhibited negative permeability and permittivity at microwave frequencies.[83] Since then, metamaterials have been explored extensively for a variety of applications in optics,[84] photonics,[85] energy harvesting,[86] sensing,[87] imaging,[88] and spectroscopy.[89] Compared with conventional SPR-based methods, metamaterials can be more easily fabricated through nanolithography techniques.[78] For periodic arrays of metamolecules, near- and far-field coupling is utilized to generate resonance with a high-quality factor (Q-factor). This breaks the damping limit of a single metamolecule in the dipole approximation,[90] thus making such arrays promising candidates for biosensing applications.[78]

2.4 Surface enhanced Raman spectroscopy (SERS) mechanism

SERS is a highly analytical tool[91,92] that has many applications in the field of diagnostics.[93] It can be used to enhance weak Raman signals of analytes through the use of plasmonic nanostructures.[94–96] Raman spectroscopy evaluates the vibrational and rotation modes of biomolecules through the analysis of inelastic Raman scattering of a laser beam.[94] Specifically, metallic nanostructures possess a localized electromagnetic field as a result of LSPR, which affects the Raman signal of an active analyte in close proximity to the nanostructure by enhancing the Raman scattering cross-section.[95] Overall, SERS shows a broad range of benefits, such as high selectivity due to the unique fingerprint signatures of analytes, easy sample preparation, high possibility of single-entity detection, high throughput, and PoC applicability by using available Raman probes.[91,92]

2.5 Surface plasmon resonance imaging (SPRi)

Surface plasmon resonance imaging (SPRi) is a real-time optical detection technique that monitors and analyzes biomolecular interactions without using any labels. While SPR and SPRi share similar detection principles, the latter provides high-throughput biosensing or screening capabilities.[97–100] The most commonly used experimental setup for SPRi is based on Kretschmann geometry.[97,100] By using, for instance, the changes in reflectivity of a thin gold film that occur upon analyte absorption, SPRi measurements allow for monitoring tens, hundreds, or even thousands of interactions simultaneously.[101] The combination of LSPRs that are obtained by nanoparticles close to the metallic surface and SPRs has been shown to enhance SPRi sensitivity in viral diagnostics.[99,100] SPRi biosensors have been demonstrated so far based on angles, wavelengths, phases, and polarization interrogations.[97–100] Angle-resolved interrogation mode, for example, continuously scans the incident angle with a fixed wavelength, while wavelength interrogation mode fixes the incident angle, whereas the SPR spectral profile and dip can be obtained by scanning the incident wavelength.[97–100] Consequently, SPRi configurations provide a variety of applications for molecular sensing, healthcare testing and environmental screening with high throughput characteristics.[97–100]

2.6 Plasmonic optical fibers

Generally, convection optical fibers are made of silica glass and have a solid core surrounded by a slightly lower refractive index cladding.[102–105] By using the total internal reflection effect, they can guide light within the core. On the other hand, plasmonic fiber-optic biosensors rely on a thin metallic film or nanostructure along the length of the sensing area to generate SPR or LSPR.[106] Therefore, part or all of the fiber cladding can be removed via chemical etching or by side-polishing methods, and nanoparticles or nanofilms can be deposited. Several optical fiber configurations such as unclad fibers, side-polished (or D-shaped) fibers, tapered, and U-shaped fibers have been demonstrated for sensing applications.[106–109] As a label-free method, these plasmonic biosensors detect biomolecular interactions with high sensitivity and low levels of detection (LOD). Their broadband operation, along with their structural flexibility and nanomaterial functionalization, makes plasmonic optical fiber-based biosensors ideal for real-time and in situ biosensing and healthcare applications.[106,107,109]

2.7 General characteristics of plasmonic biosensors

The basic components of a biosensor are illustrated in Fig. 3(a) and consist of the target analyte bound to the bioreceptor, the transducer, which converts the signal into a measurable quantity, and the reader device, which generates the results[110,111] (detailed descriptions of these components are available elsewhere and are beyond the scope of this work[110,111]). In addition, chemical activation of the surface is crucial to improve the sensing efficiency of single virus particles. Some important features of analyte–receptor coupling on the plasmonic surface are shown in Fig. 3(b). Typically, in affinity-based plasmonic biosensors, surfaces are activated by biological receptors, such as antibodies, nucleic acids, cell membrane receptors, specifically designed peptides, aptamers, or molecularly imprinted polymers (MIPs).[112] These biological entities show great affinity and specificity for certain analytes, allowing for the selective
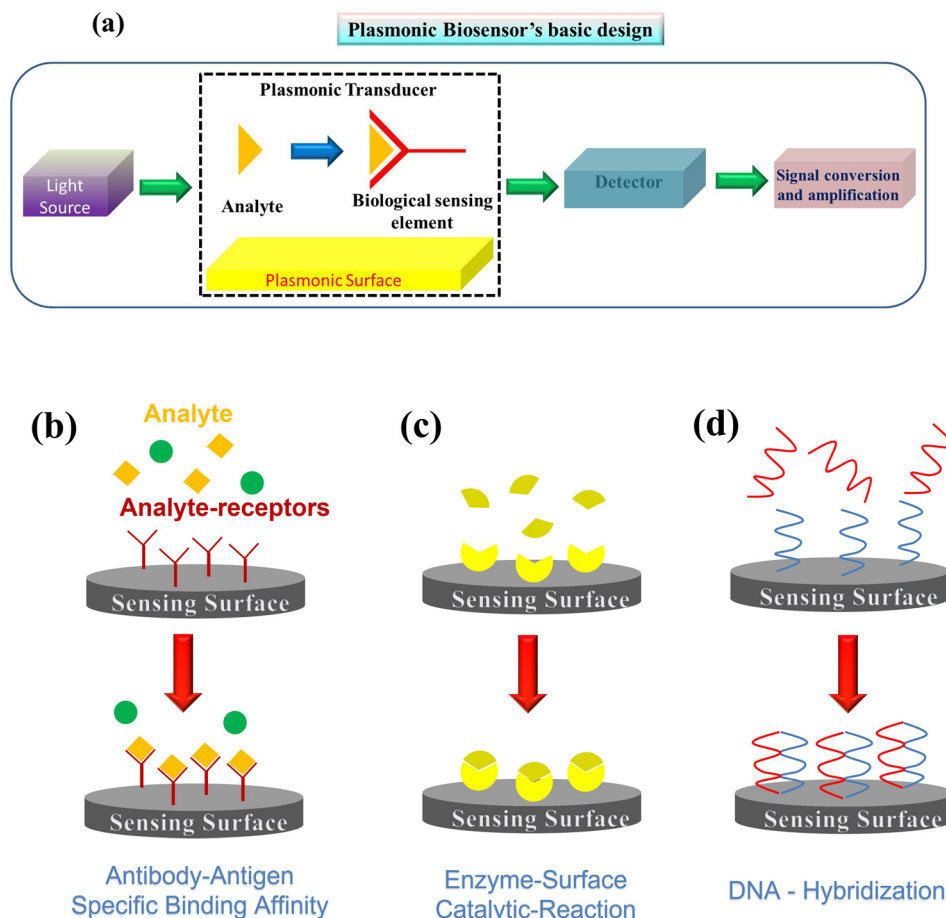
Fig. 3 (a) Schematic illustration of a plasmonic biosensor that translates the capture of the analyte to a measurable alteration of light intensity or resonance shift. Analyte–receptor coupling mechanisms on the plasmonic biosensor surfaces include (b) antibody–antigen binding, (c) enzyme–surface catalytic reactions, and (d) DNA hybridization.

capture of the target with high sensitivity from complex biological samples. In the following section, we will focus on several parameters used to assess the performance of a biosensor.[110] In the context of biosensing, the most important feature of a sensor is its sensitivity, S,[110] it is described by eqn (3) and can be determined by the slope of the analytical calibration curve,

$$S = \frac{\Delta\lambda}{\Delta n} \quad (3)$$

where λ is the surface plasmon resonance and n is the refractive index of the medium in contact with the sensor surface. The magnitude of a sensor's sensitivity depends on the supporting electromagnetic mode, resonant wavelength, excitation geometry, and properties of the substrate.[113] Therefore, bulk and surface sensitivities are not necessarily linked to each other. For instance, for a thin gold film excited at a low angle using a Kretschmann configuration, a high bulk sensitivity (>5000 nm per RI unit [RIU]) can be achieved, while a simultaneous small surface sensitivity is obtained because of the high decay depth.[44] This implies that a small amount of an analyte (<10 kDa) can be easily

detected using a biosensor with a small penetration depth.[44,114]

Another key parameter is the limit of detection (LOD) or sensor resolution, which is defined as the smallest amount of analyte that can be reliably detected by a specific measurement process. It is determined by the concentration of the analyte that produces a biosensor response corresponding to the standard deviation, σ_{blank}, of the biosensor response measured with no analyte and is given by:[113,115]

$$\text{LOD} = m\frac{\sigma_{blank}}{S} \quad (4)$$

where m is a numerical factor. A typical resolution of 10^{-6} RUI has been demonstrated with gold films and a Kretschmann configuration.[116] Piliarik and Homola[117] calculated the ultimate theoretical resolution of an SPR sensor to be 10^{-7} RUI. The authors showed that such a resolution could be reached regardless of the type of SPR coupling or signal modulation by, for example, increasing the signal-to-noise ratio of the detected light using high-end optoelectronic components.[117]

The performance of a plasmonic biosensor is strongly influenced by the spectral shape and background noise of the readout system. For the spectral shape, the Q-factor is an important parameter since it is a reliable indicator of the resolution of the detector for certain analytes and is given by:[118]

$$Q = \frac{\lambda}{\text{FWHM}} \tag{5}$$

To enhance sensing performance, large Q-factor values are desirable because sharper resonance peaks with large Q-factors make it much easier to detect small RI changes.[77] For example, nanostructures that support Fano resonances lead to sharp asymmetric peaks that show up to two-fold sensitivity enhancement when compared with conventional biosensors.[119,120]

Another important characteristic of a biosensor is the figure of merit (FOM), which is the ratio between the sensitivity and full width at half maximum of the resonance spectra.[114]

$$\text{FOM} = \frac{S}{\text{FWHM}} \tag{6}$$

The FOM is a key factor for evaluating and comparing different plasmonic nanostructures with respect to their sensing potential and is dependent on the metal film, prism material, and resonance.[121] In conclusion, the optimum performance of a plasmonic biosensor should be evaluated after taking into account several factors that require carefully consideration.

3 Plasmonic biosensors

Plasmonic optical biosensor technology has emerged as a powerful diagnostic tool.[138–141] By selecting the appropriate biorecognition element, the technology can be applied to virtually any type of target molecule, from proteins, nucleic acids, bacteria, and drugs, and up to human cells,[1,43,119,142,143] while many studies have demonstrated its utility in the biomedicine and environmental fields.[30,37,89,95,115] In medicine, the accurate diagnosis of specific diseases is key for the timely and appropriate treatment and clinical management of a patient. Moreover, the rapid and early identification of certain viral diseases before the appearance of external symptomatology can also be important. This is the case with COVID-19; the availability of plasmonic biosensors for the rapid and accurate detection of severe acute respiratory syndrome coronavirus 2 (SARS-CoV-2) may be useful for massive population screening, early detection of infected patients, and more efficient management of the pandemic.[1,2,4,144] Owing to the versatility of plasmonic biosensors, the detection process can be modified. For example, the use of genomic RNA sequences of the virus target, instead of viral antigens, has enabled the rapid development of specific reverse transcription RT-PCR-based genomic assays.[1] Hence, plasmonic biosensors can be applied to the direct and label-free detection of viral RNA by designing and immobilizing single-stranded DNA probes, as receptors, with complementary sequences to specific SARS-CoV-2 gene fragments on the sensor surface.[1] Moreover, the sensitivity and specificity for SARS-CoV-2 could be increased with the combination of several probes targeting genes of the same virus.[1] Henceforth, in this review, we will discuss recent plasmonic biosensor platforms for virus detection, with an emphasis on SARS-CoV-2 (Table 1).

Table 1 Overview of plasmonic-based biosensors for virus detection

| Structure	Virus detected	Detection format	LOD sensitivity	Ref.
Ag/Au (35 nm/10 nm) chips	Avian influenza H7N9	Monoclonal antibody (IgM)	144 copies per mL	122
Cr/Ag/Au (3 nm/40 nm/10 nm) chips	Human enterovirus 71	Enterovirus antibody	67 virus particles (vp) per mL	123
Cr/Au (2.5 nm/47 nm) chips	H1N1, RSV, adenovirus, SARS	PCR amplified viral bodies	0.5 nM for adenovirus/2 nM for SARS	124
Au SPR chip	Ebola virus	Monoclonal antibodies	0.5 pg mL^{-1}	125
Biacore X bare gold chip	HIV	Hairpin DNA, capture probes	48 fM	126
Array of Au nanoprism	Rotavirus	Rotavirus capsid (2B4) antibody	126 ± 3 PFU mL^{-1}	127
Array of Au nanodisks and nanodots	Ebola virus	A/C protein	220 fg mL^{-1}	18
Planar toroidal gold metamaterial	Zika virus	Immobilized antibody	5.81 GHz log(pg mL^{-1})$^{-1}$	128
Au toroidal metasensor	SARS CoV-2	SARS antibody	4.2 fmol	129
Au nanospikes	SARS CoV-2	SARS antibody	0.08 ng mL^{-1}	13
Au nano-island layer	SARS CoV-2	Thiol cDNA receptor	0.22 pM	130
Hetero-assembled Au nanoparticles layer	Hepatitis B virus	Hepatitis antibody	100 fg mL^{-1}	131
Au spike-like nanoparticles	Avian influenza virus	DNA–hemagglutinin binding aptamer	1 pg mL^{-1}	132
Au (~20 nm) particles	Norovirus	Norovirus recognizing affinity peptide	9.9 copies per mL	133
Bioconjugated Au nanoparticle (10–15 nm)	Dengue and West Nile viruses	Antiflavivirus 4G2 antibody	10 plaque-forming units (PFU) per mL	134
SiO$_2$/Au particles (4 nm/100 nm)	Zika virus	Anti-Zika (NS1) antibody	10 ng mL^{-1}	135
Ag particles (20–80 nm)	Dengue virus	NS1 antibody	0.06 µg mL^{-1}	136
Au particles (40 nm)	SARS CoV-2	Nucleocapsid (N) protein	150 ng mL^{-1}	137
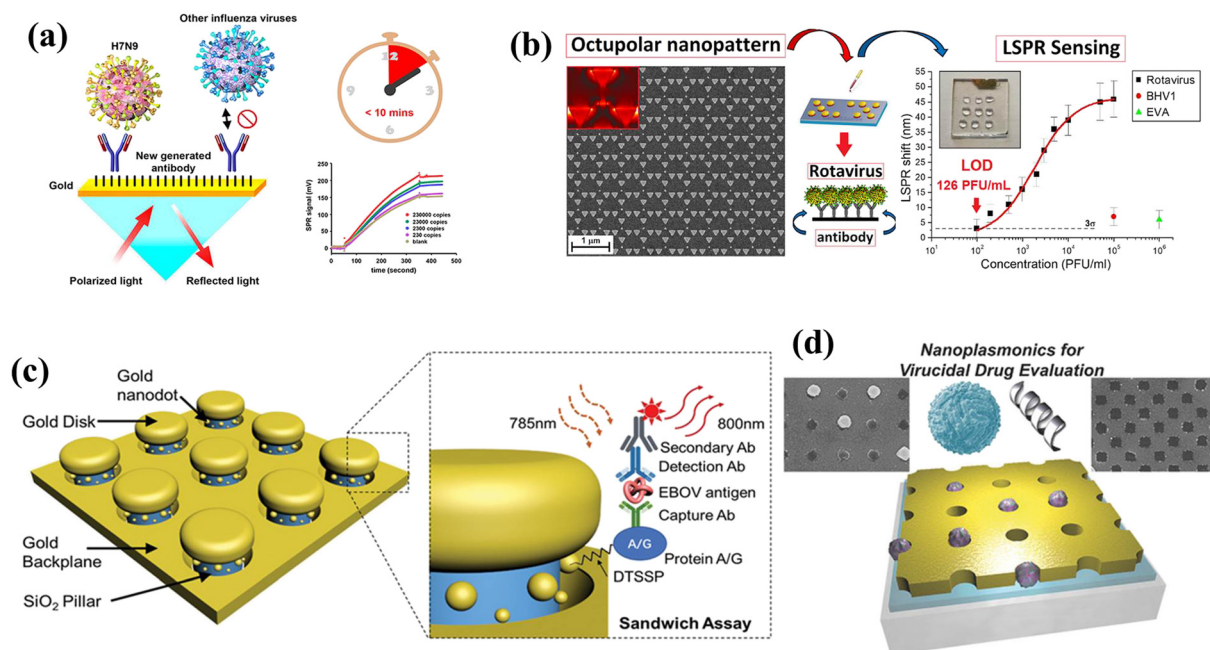
Fig. 4 (a) Schematic of a plasmonic biosensor used to identify avian influenza H7N9. A bare Ag/Au chip is cleaned before surface functionalization with self-assembled monolayers. The capture antibody, at a concentration of 10 μg mL^{-1}, is covalently immobilized to the reaction spot of the chip (reproduced with permission from ref. 122). (b) Left: Scanning electron microscopy images of the octupolar geometry-based Au nanostructure used for rotavirus detection. The minimum interparticle distance between two unit cells is 25 nm. Right: Average LSPR peak shift (black square) and Langmuir isotherm fitting (red line) for various concentrations of rotavirus in distilled water (reproduced with permission from ref. 127). (c) Schematic of a nano-antenna array for Ebola virus detection. The gold nanodisks and backplane are separated by SiO$_2$ nanopillars, forming nanocavities. Gold nanoparticles are present on the SiO$_2$ pillar surfaces, where the localized electromagnetic field around the nanostructure is highest (reproduced with permission from ref. 147). (d) Schematic of a periodic gold nanohole array that was designed in order to selectively capture lipid vesicles and virus particles inside the nanoholes. The 10 × 10 mm gold nanohole array was formed on a glass substrate by the template-stripping method. An optical adhesive layer is present between the gold and glass (reproduced with permission from ref. 148).

3.1 Biosensing using plasmonic nanostructures

The first implementation of plasmonic label-free biosensors for influenza virus detection was reported 25 years ago.[145] Since then, researchers have developed a variety of biosensor assays for rapid virus detection and quantification based on plasmonic technologies.[146] Chang *et al.* reported a simple strategy for avian influenza A (H7N9) virus detection using an intensity-modulated SPR biosensor integrated with a monoclonal antibody (Fig. 4(a)).[122] Specifically, the authors employed a Kretschmann configuration using an Ag/Au (35 nm/10 nm) chip to increase the selectivity for the virus. They noted an LOD of 144 copies per mL, which indicated a sensitivity 20-fold higher than with target-captured ELISA using antibodies, and better than conventional RT-PCR tests.[122] Furthermore, they evaluated their configuration using mimic clinical specimens containing the H7N9 virus mixed with nasal mucosa from patients with flu-like symptoms and noted a detection limit of 402 copies per mL, which was far superior to conventional influenza detection assays, and a rapid testing time of under 10 min.[122] Likewise, Prabowo *et al.*[123] demonstrated a portable SPR biosensor for the quantification of enterovirus antibodies, which showed a detection limit of 67 copies per mL. In another study, an SPR-based biosensor was used to detect nine common

respiratory viruses with an LOD of 2 nM for SARS,[124] while an SPR chip developed to detect the Ebola virus showed a sensitivity of 0.5 pg mL^{-1}.[125] The authors modified a gold chip with 4-mercaptobenzoic acid and used three monoclonal antibodies of Ebola virus to study the efficiency based on the affinity constant.[125]

A biosensing platform developed by Diao *et al.*[126] based on the Biacore X analytical system was able to obtain 48 fM of HIV-1-related DNA using entropy-driven strand displacement reactions (ESDRs) as an isothermal, label-free nucleic acid amplification technique. The authors developed a sensitive SPR biosensing strategy for enzyme and label-free detection based on DNA nanotechnology.[126] The whole detection process was accomplished in 60 min with high accuracy and reproducibility.[126] The authors noted that the observed biosensing performance could be attributed to the perfect combination of a hairpin probe, ESDR circuit, and DNA tetrahedra on the SPR biosensing chip.[126] Another SPR device has been demonstrated to investigate antigen–antibody interactions of chicken infectious bronchitis coronavirus.[149] The authors utilized a prism configuration using a 50 nm Au film to increase the specificity of the virus.[149] Compared with the expected response rate, the SPR sensor had much smaller differences (up to 6.3 times) between specific and non-specific interactions.[149] The effect

of buffer acidity changes was also investigated, showing a six-fold reduction in non-specific interactions.[149]

A two-dimensional octupolar geometry-based gold nanostructure was fabricated by Rippa et al.[127] to detect ultrasmall concentrations of rotavirus, which is the main cause of childhood viral gastroenteritis in humans (Fig. 4(b)). Specifically, the authors designed an array of units comprising three large identical triangular gold nanoprisms (side length, 200 nm) and one smaller inner prism (side length, 80 nm), with a 25 nm separation between adjacent units.[127] An LOD of 126 ± 3 PFU mL^{-1} using a very low sample volume (2 μL) was estimated. In addition, the authors evaluated their plasmonic biosensor with two more viruses (bovine herpesvirus [BHV1] and equine viral arteritis [EVA]) to confirm its sensitivity and specificity. A maximum LSPR peak shift of 7 nm from a concentration of 1×10^5 PFU mL^{-1} for BHV1 was measured, while a maximum shift of 6 nm was observed for EVA.[127] A microfluidic polymerase chain reaction with a gold nanoslit-based SPR sensor was fabricated to detect the DNA sequence of latent membrane protein 1 (LMP1) from Epstein–Barr virus (EBV)-positive cells.[150] The device was divided into the PCR microchannel and gold nanoslit of 80 nm width.[150] The microfluidic PCR was integrated with the nanoslit SPR chip, using heat-resistant double-sided tape.[150] Finally, the sensor was evaluated using samples from nasopharyngeal cancer patients and completed the analytical procedure in 36 min, with an LOD of 10^{-11} g mL^{-1}.[150]

Recently, an array of gold nano-antennas that uses a sandwich immunoassay format has been fabricated for single-molecule detection of Ebola virus antigens (Fig. 4(c)).[147] The nano-antenna consists of SiO$_2$ nanopillars bound to gold nanodisks and nanodots, which enhance the fluorescence signal through the formation of nanocavities.[147] The authors used a thiol–gold link and a protein A/C layer to simultaneously functionalize the surface of the nanopillars and to prevent signal losses on the gold surfaces.[147] They noted a detection sensitivity for the Ebola virus soluble glycoprotein in human plasma of 220 fg mL^{-1}; this was a significant improvement over the recommended immunoassay test for Ebola virus antigens.[147] In addition, the interaction of light with the periodic array of nanoholes enabled the extraordinary optical transmission effect,[151] which enhanced the transmission of light at specific wavelengths. These spectral characteristics have facilitated the development of high-sensitivity plasmonic biosensors that can be integrated with microfluidics. A metallic nanohole-based assay was developed[148] to capture single virus-like particles (Fig. 4(d)). The diameter of the nanoholes was chosen to fit the size distribution of virus particles that had been treated with a virucidal drug candidate.[148] The sensing performance of the platform was evaluated by monitoring resonance shifts for the virucidal-induced capture of single virus-like particles, showing a minimum RI resolution of 5.5×10^{-5} RIU.[148] The authors noted high RI sensitivity in the functionalized nanoholes with a low surface coverage when compared with non-functionalized nanoholes.[148]

Since terahertz waves are non-ionizing and harmless to organic tissues and biomolecules, they may become increasingly attractive for biomedical applications.[156] A terahertz gold metasensor was designed for Zika virus envelope protein detection.[128] Based on toroidal metamaterial properties, these devices support resonances that possess much higher sensitivity to RI perturbations in the surrounding media.[82,83] The toroidal metamaterial consisted of an array of mirroring asymmetric split resonators and had the ability to support a Q-factor[128] around 30. By measuring the shift of the toroidal dipolar momentum, the authors determined the LOD and sensitivity of the metasensor to be 560 pg mL^{-1} and 5.81 GHz log(pg mL^{-1})$^{-1}$, respectively, for a variety of Zika virus concentrations.[128]

3.1.1 Plasmonic nanostructures for SARS-CoV-2 detection. Ahmadivand et al. demonstrated femtomolar-level detection of the SARS-CoV-2 S protein using toroidal gold metasensors.[129] The authors improved the binding properties of the device by functionalizing gold nanoparticles with antibodies for the S protein, resulting in an LOD of 4.2 fmol mL^{-1}.[129] A low-cost plasmonic sensor consisting of an Au–TiO$_2$–Au nanocup array was demonstrated which permitted observation of the plasmon resonance wavelength and intensity change of S protein capturing events by utilizing the extraordinary optical transmission effect in transmission light spectroscopy.[157] The authors achieved an LOD of 370 virus particles (vp) per mL with a virus concentration in the range of 0–10^7 vp mL^{-1}.

A plasmonic nanohole array with S protein antibodies immobilized on the surface was fabricated[152] to detect a broad range of pathogens in a typical biology laboratory setting (Fig. 5(a)). By capturing the S proteins, whole virus particles could be suspended in the nanohole array, which resulted in a red-shift of the resonance.[152] A plasmonic microfluidic biosensing platform was developed by Funari et al. who demonstrated the utility of electrodeposition-based gold nanospikes combined with optical probes.[13] Based on local RI changes caused by the interaction of the SARS CoV-2 S protein and antibodies in the diluted human serum, a shift of the LSPR resonance peak was detected, with a detection concentration of 0.08 ng mL^{-1}.[13] The authors noted that the proposed platform could complement existing serological assays and improve COVID-19 diagnosis.[13] A dual functional plasmonic detection platform that combines the plasmonic photothermal[33] and LSPR effects has been reported for SARS-CoV-2 detection[130,153] (Fig. 5(b)). Two-dimensional gold nano-islands functionalized with RdRp-COVID cDNA (RdRp-COVID-C) receptors permit the selective detection of RdRp-COVID-C through DNA hybridization, giving an LOD for the cDNA of 0.22 pM. This provides a new approach for SARS-CoV-2 detection.[130,153]

A label-free detection assay scheme based on an antifouling polymer brush biointerface prepared on a gold-
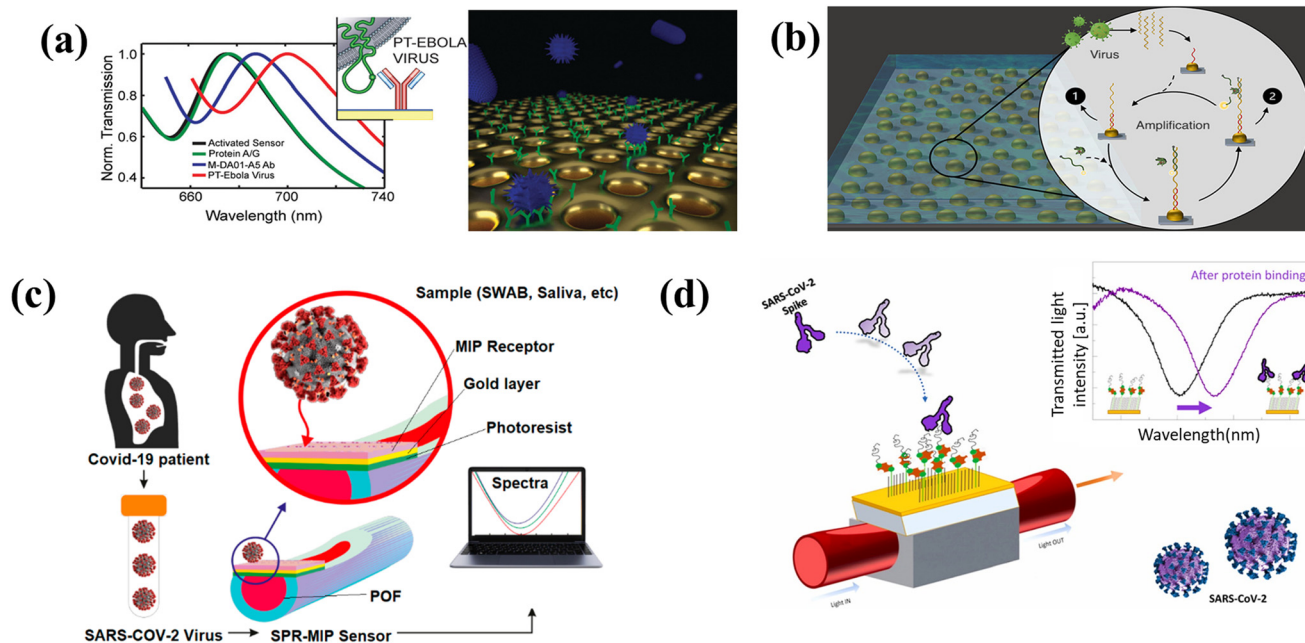
Fig. 5 (a) Schematic of the thermoplasmonic-assisted dual-mode approach. Amplification-free-based direct viral RNA detection and amplification-based cyclic fluorescence probe cleavage detection are combined to provide SARS-CoV-2 detection within 30 min (reproduced with permission from ref. 152). (b) A label-free optofluidic nanoplasmonic sensor that can detect vesicular stomatitis virus and pseudotyped Ebola virus from biological media with little to no sample preparation (reproduced with permission from ref. 153). (c) Schematic of a biosensor based on a plasmonic plastic optical fiber coupled with a novel type of synthetic molecularly imprinted polymer (MIP) receptor for the specific recognition of subunit 1 of the SARS-CoV-2 spike (S) protein (reproduced with permission from ref. 154). (d) Biosensing configuration based on an SPR D-shaped plastic optical fiber integrated with an aptamer for the recognition of the receptor-binding domain (RBD) of the S glycoprotein of SARS-CoV-2 (reproduced with permission from ref. 155).

coated piezoelectric quartz crystal microbalance chip was fabricated to enable the quantitative analysis of N-protein of SARS-CoV-2.[158] This device improved the bioassay sensitivity to a clinically relevant LOD of 1.3×10^4 PFU mL^{-1} within a detection time of only 20 min.[159] A customized SPR serological biosensor based on the Kretschmann configuration incorporated with microfluidic components in a compact and user-friendly platform was demonstrated for identification and quantification of SARS-CoV-2 antibodies in clinical samples.[160] By using polyclonal antibodies, this portable plasmonic device has diagnostic sensitivity (99%) and specificity (100%) for clinical COVID-19 positive and negative samples.[160] Ansah *et al.* introduced a methodology for the synthesis of interior hotspots templated with protein for label-free and on-site SERS detection of the virus.[161] Specifically, the structure consisted of Au nanocavity electrode (AuNC) with a large surface area, high aspect ratio, and negligible background noise fabricated on a Si substrate.[161] A supporting electrolyte solution of NaCl, protein and Au precursor was used during electrochemical deposition to synthesize the core–shell structure that encapsulated the lysate protein of SARS-CoV-2 (SLs) protein.[161] The whole process was carried out under an applied potential of 0.3 V and illumination of a laser beam at 785 nm.[161] They authors detected SLs with an LOD value of 10^{-1} PFU mL^{-1}.[161] An inverted gold pyramidal metasurface was designed, fabricated, and evaluated for label-free

hepatitis A virus (HAV) detection by employing SERS.[162] The authors fabricated 300×300 μm^2 Au nanostructures based on periodic arrays of inverted pyramidal nanoholes (PNHs) by using an EBL method.[162] The PNHs are equilateral triangular based (side size of 390 nm) and arranged in a triangular geometry.[162] For this study, the 785 nm excitation wavelength was used to test the SERS performances of the PNHs.[162] The HAV was detected at a concentration of 10^3 PFU mL^{-1}, corresponding to 13 pg mL^{-1}.[162]

3.2 Biosensing using plasmonic two-dimensional materials

A number of studies on two-dimensional (2D) layered materials for biochemical sensing applications have exploded since the synthesis of graphene.[163] In a variety of healthcare applications, these materials (*e.g.* graphene, transition metal dichalcogenides, graphitic and transition-metal carbides) can serve as active sensing elements or supporting substrates due to their electrical, optical, electrochemical, and physical properties, which are often tunable.[164–167] By reducing their geometrical dimensions, 2D-materials enhance plasmonic field confinement and enable the excitation of plasmons, excitons, and phonons to demonstrate new biosensing functionalities.[166–168] In the literature, several review papers[164,165,169,170] have addressed the role of 2D-materials in developing detection platforms with high sensitivity and selectivity towards the target analyte.

For example, graphene oxide (GO)-based fluorogenic peptide probes were designed to allow the differentiation of Ebola virus from Marburg virus which has a similar capsid protein composition as well receptor-extensive vesicular stomatitis virus.[171] The authors used an array of three fluorescent peptide fragments with modest affinity and selectivity for these three viruses.[171] By increasing the concentration of the peptide probes and applying statistical analysis, the authors determined the characteristic patterns for each virus in a simple way without the need for specific peptide ligands.[171] A reduced-GO-based SPR sensor functionalized with specific antibodies was developed for the detection of dengue virus for concentrations of 0.1 pM.[172] Peng et al. demonstrated a sensing platform based on ultrathin 2D-MXene Ti_3C_2 nanosheets for the detection of PVR-amplified HPV-18 DNA from cervical scrape samples obtained from human papillomavirus infected patients.[173] The authors noted high sensitivity and selectivity for HPV-18 determination, with an LOD of 100 pM.[173] Molybdenum disulfide (MoS_2) nanostructures[166,167,174,175] were synthesized for nanomedicine and biosensing applications.[176,177] For instance, a MoS_2-based biosensor was developed to quantify hepatitis C virus gene (HCV).[175] The authors employed an isothermal enzyme-free hybridization chain reaction for DNA amplification to form long dsDNA to explore the plasmon effect of MoS_2 nanosheets.[175] The proposed biosensor detected HCV gene from 0.5 pmol L^{-1} to 1 nmol L^{-1} with an LOD of 0.17 pmol L^{-1}.[175]

3.3 Two-dimensional (2D) materials for SARS-CoV-2 detection

A 2D heterostructure based on $PtSe_2$/graphene was attached to the gold film of the SPR biosensor for the rapid detection of the coronavirus.[178] In this work, the performance of the biosensor was investigated with three different ligand–analytes: (i) the monoclonal antibodies as the ligand and the coronavirus spike receptor-binding domain (RBD) as the analyte, (ii) the virus spike RBD as the ligand and the virus anti-spike protein (IgM, IgG) as the analyte, and (iii) the specific RNA probe as the ligand and the virus single-stranded RNA as the analyte.[178] The heterostructure $PtSe_2$/graphene provided an increased surface area for better absorption of the target analyte and enhanced the sensitivity of the biosensor. The authors noted a sensitivity of 833 THz RIU^{-1} in SPR frequency for COVID-19 virus spike RBD detection.[178] One year later, the same research group proposed a graphene-coated BK_7/WS_2/Au/$BaTiO_3$ sensor for detecting SARS-CoV-2 virus at an early stage.[179] The authors noted a sensor angular sensitivity of 230.7 deg RIU^{-1} for detecting the SARS-CoV-2 whole virus and an angular sensitivity of 227.6 deg RIU^{-1} for the detection of monoclonal antibodies against the SARS-CoV-2 virus.[179] In another study, selective detection of COVID-19 virus is demonstrated by using an antibody functionalized graphene material as a Raman transducer platform.[180] The phononic energy of graphene is strongly influenced by the change in its doping

level when an analyte molecule is attached.[180] The authors noted that when negatively charged COVID-19 spike RBD proteins are bonded to CoV-2 spike RBD antibody functionalized graphene, a blue shift in the phonon vibration mode peak results from the p-doping of the p-type graphene.[180] The achieved LOD with this graphene-based phononic biosensor was 3.75 fg mL^{-1} and 1 fg mL^{-1} of spike virus protein in artificial saliva and buffer solution, respectively.[180]

3.4 Biosensing using plasmon-based optical fibers

In the past few decades, optical fibers have evolved from an optical transmission waveguide to important components of applications ranging from small particle manipulation[102–105,181] to medical imaging.[182] In the past decades, a new class of optical fiber sensors based on SPR has been added to the family of PoC devices.[183] Plasmonic fiber-optic biosensors offer an interesting alternative to classical prism-based configurations and are advantageous in terms of flexibility and cost. Plasmonic optical fiber platforms have provided miniaturized sensing approaches for the determination of clinical biomarkers.[184]

An SPR-based optical fiber device has been developed for the analysis of avian influenza virus subtype H6.[185] The SPR-based optical fiber consists of a 40 nm thin gold film and a side-polished structure.[185] To optimize the self-assembled monolayers and subsequent antibody functionalization, the detection surface of the SPR-based optical fiber was modified with plasma at low temperature, which rendered better results than chemical modification.[185] The binding interaction between immobilized antibodies and antigens on the cell surface was evaluated with 10^4 to 10^8 embryo infectious dose $(EID)_{50}$ per 0.1 mL of virus, leading to an LOD of 5.14×10^5 EID_{50} per 0.1 mL and an average response time of 10 min.[185] By combining the optical properties of LSPR nanostructures with the total internal reflection of optical fiber configurations, better spatial sensitivity can be achieved. For example, the integration of gold nanorods into a fiber-optic platform permitted the development of an immunosensor for the determination of Cymbidium mosaic virus and Odontoglossum rings spot virus[186] in plants. To achieve direct sensing of the analytes, gold nanorods were employed to generate a near-infrared sensing window to solve the color interference issue of sample matrices.[186] The optical fiber LSPR-based platform provided an LOD of 48 pg mL^{-1}, while the RI resolution was 8×10^{-6} RIU.[186] The authors noted that the improvement in sensitivity in comparison with ELISA was attributed to the properties of nanorods, which simultaneously prevented the color interference of similar-sized nanospheres.[186] A tilted fiber grating surface coated with gold nanoparticles has been demonstrated for the detection of Newcastle disease virus (NDV).[187] Modification of the fiber cladding with gold nanoparticles (with an average diameter of 80 nm) enhanced the sensitivity as a result of the LSPR field, while activation

of the nanoparticles with staphylococcal protein A improved the bioactivity of anti-NDV monoclonal antibodies by up to ten times compared with that of a tilted fiber grating without gold nanoparticles.[187] Monitoring of resonance wavelength red-shifts showed a minimum detectable amount for virus of approximately 5 pg; this is slightly better than that achievable by RT-PCR (10 pg).

3.4.1 Plasmonic optical fibers for SARS-CoV-2 detection. During the recent pandemic, a plasmonic fiber optic absorbance biosensor was successfully fabricated to detect the SARS-CoV-2 nucleocapsid (N) protein.[188] The integration of gold nanoparticles into a multimode U-bent optical fiber permitted the detection of the N protein in a patient's saliva sample within 15 min.[188] An alternative biorecognition system based on aptamers immobilized on gold nanorods embedded in D-shaped optical fibers was also fabricated for the detection of the SARS-CoV-2 S protein (Fig. 5(c)).[154] The viral protein was detectable at an LOD of 37 nM and resonance shifts of 3.1 nm, thereby providing the ability to detect small viral concentrations.[154] The same group fabricated a synthetic MIP receptor, which was incorporated into a 60 nm thick gold film D-shaped optical fiber, for the identification of SARS-CoV-2 (Fig. 5(d)).[155] In this work,[155] the authors noted that the sensitivity of the proposed plasmonic biosensor was higher than RT-PCR with a response time of about 10 min. A photonic quasi-crystal fiber (PQCF)-based plasmonic platform was designed to provide a theoretical sensitivity of 1172 nm RIU^{-1} for the detection of SARS-CoV-2 within saliva.[189] The PQCF consisted of 280 nm diameter air holes and a 300 nm diameter gold ring around one air hole near the core of a lattice with a 500 nm period.[189] Sensors used for detecting analytes should be capable of biosensing and amplification of targeted analytes at low concentrations. Therefore, Yosra *et al.* analyzed the sensitivity and resolution of an optical fiber-based system with gold–silver alloy nanoparticles embedded in its core and covered by a layer of graphene.[190] The authors[190] showed that the system had a maximum sensitivity of 7100 nm RIU^{-1}, FOM of 38.8 RIU^{-1}, and signal-to-noise ratio of 0.38. Moreover, Wu *et al.*[191] showed that the combination of metallic nanostructures with graphene can provide better biological sensing because of the adsorption of analytes to the graphene through π–π stacking. Hence, the modification of the plasmonic optical fiber with graphene layers may improve further the performance and detection ability of future biosensors.

3.5 Biosensing using plasmonic nanoparticles

The characteristics of metal nanoparticles have found the greatest use in LSPR biosensing, with several applications utilizing this technique.[144,192–194] For example, a sandwich immunoassay with gold nanoparticles was demonstrated to detect the hepatitis B virus (HBV) surface antigen (HBsAg).[131] For this purpose, a glass substrate was fabricated with synthesized gold nanoparticles (AuNPs) of three different sizes (15, 30, and 50 nm) and conjugated with an anti-HBsAg antibody to detect the target antigen.[131] After 10 min, a second layer of AuNPs conjugated with the anti-HBsAg antibody was added to obtain a hetero-assembled chip, the LOD of which was 100 fg mL^{-1}.[131] Takemura *et al.* used the LSPR signal from Ab-conjugated thiol-capped AuNPs to amplify the fluorescence intensity signal of quantum dots for the detection of nonstructural protein 1 (NS1) of the Zika virus.[195] Their biosensor had a wide detection range of 10–10^7 RNA copies per mL and maintained its specificity with human serum.[195] Chowdhury *et al.* also developed a biosensor using AuNPs and CdSeTeS quantum dots to identify the serotypes of dengue virus.[196] The biosensor had LOD at the femtomolar level and was successfully applied to RNA extracted from dengue virus culture fluids.[196] Lee *et al.* constructed a label-free biosensor for avian influenza virus (H5N1) using hollow spike-like AuNPs and a three-way DNA junction.[132] To achieve multifunctionality, each piece of DNA was tailored to aptamers specific for the hemagglutinin (HA) protein of the virus, fluorescence dye, and thiol group. The sensor detected the HA protein of H5N1 in phosphate-buffered saline and chick serum with an LOD of 1 pM.[132] Heo *et al.* fabricated gold nanoparticles with an approximate average size of 20 nm to detect human norovirus.[133] The authors' novel sensing approach utilized noroviral protein-recognizing affinity peptides, which are relatively cost-effective compared with antibodies, to bind noroviral proteins.[133] They noted an LOD of the capsid protein of 9.9 copies per mL.[133]

AuNPs or roughened gold surfaces are also widely used in SERS spectroscopy because of their LSPR properties.[144] Paul *et al.* developed an antibody-conjugated AuNP-based SERS probe for the identification of mosquito-borne viruses.[134] They successfully detected dengue virus type-2 and West Nile virus at a low concentration of 10 PFU mL^{-1}.[134] Camacho *et al.* designed SERS nanoprobes using gold shell-isolated nanoparticles, which contained 100 nm gold nanoparticles and 4 nm silica shells. The silica shells modified with Nile blue functioned as the Raman reporter.[135] This configuration was irradiated with a 633 nm wavelength laser beam, and the Raman signal was recorded by a mapping process. The nanoprobes successfully detected Zika virus at a very low concentration (around 10 ng mL^{-1}) and without any cross-reactivity with dengue virus.[135] Luan *et al.* developed a stable and bright fluorescent plasmonic nanoscale construct that consisted of a bovine serum albumin (BSA) scaffold with approximately 210 IRDye 800CW fluorophores, a polysiloxane-coated gold nanorod acting as a plasmonic antenna, and biotin as a high-affinity biorecognition element.[197] This configuration was able to improve the LOD of fluorescence-linked immunosorbent assays by up to 4750-fold, shorten the overall assay time (to 20 min), and used lower sample volumes.[197] The authors attributed this improvement in sensitivity to the BSA blocking method, in which BSA acts as a blocking agent to minimize non-specific binding of the plasmonic fluorophore to arbitrary surfaces

and biomolecules. In another study, an ATR-LSPR-based optical platform was employed to demonstrate the detection of ChiLCVa plant virus using its complementary DNA sequence as a receptor.[198] Gold nanoparticles of 50 nm diameter were immobilized on a functionalized coverslip surface by the ATR-configured evanescent wave-based LSPR absorption method.[198] The sensor's LOD was 1.0 μg ml^{-1} for the plant viral DNA sample, while unique binding dynamics were observed compared to non-specific DNA.[198]

Compared with gold nanoparticles, silver nanoparticles display a higher efficiency of LSPR excitation and a wider wavelength range.[199] Moreover, silver nanoparticles have sharper LSPR bands, are less dissipative, and perform better in SERS.[193] However, there are fewer studies on AgNPs than AuNPs as plasmonic biosensors. One reason behind this may be that AgNPs display toxicity[200,201] and antiviral effects.[202,203] Another reason is that bare AgNPs are not as stable as AuNPs because of quicker oxidation.[204] To deal with these drawbacks, AgNPs are usually coated with different materials.[205] The thickness and the type of coating material greatly influence the optical properties of AgNPs. A thermally annealed thin silver film deposited onto a silicon substrate was used to detect the NS1 antigen of dengue virus in whole blood.[136] After the annealing process, silver nanoparticles with diameters from 20 to 80 nm were generated and with inter-structural spacing ranging from a few tens to about 100 nm.[136] The authors determined the system to have an RI sensitivity of 10^{-3}, while an increase in absorption and a red-shift of 108 nm of the peak absorption wavelength were observed with antigen binding.[136] The sensitivity of this configuration was found to be 9 nm μg^{-1} mL^{-1}, and the LOD was 0.06 μg mL^{-1}. Hong et al. developed hybrid slot antenna structures with silver nanowires in the terahertz frequency range to detect bacteriophage PRD1 and obtained an enhancement factor of 2.5 for a slot antenna width of 3 μm.[206]

A SERS platform has been used to detect HBV.[207] The authors used a standard, label-free Ag nanoparticle solution as the SERS-active substrate to test blood serum samples from HBV patients and healthy volunteers.[207] The SERS spectra of the serum samples from both the infected patients and healthy volunteers were compared by employing linear discriminant analysis.[207] Using this approach, a SERS spectrum was produced in 10 min for each sample and with a diagnostic sensitivity of 91.4%, indicating the great potential of this platform for a quick, non-invasive, label-free diagnostic method through the implementation of principal component analysis (PCA).[207]

3.5.1 Metallic nanoparticles for SARS-CoV-2 detection. A SERS platform consisting of heteronanostructures that control the coupling distance between the two tethered metallic nanostructures for ultrasensitive and highly selective nucleocapsid (N-cDNA) gene detection of SARS-CoV-2 was reported.[159] Specifically, the sensing platform consisted of a silicon wafer that is modified with bovine serum albumin-reduced graphene oxide and N gene probing oligo-conjugated

AuNPs.[159] Superparamagnetic iron oxide nanoparticles were modified with another N-cDNA probing sequence to sandwich the immobilized N-cDNA on the sensing substrate.[159] According to the authors, SERS signals increased by 10 times in the detection limit from 1 fM to 100 aM.[159] A plasmonic biosensor for thickness-sensing detection via utilizing the distance-dependent electromagnetic coupling in sandwiched Au nanoparticles and Au film structures was demonstrated for naked-eye detection of antibodies against SARS-CoV-2.[208] This assay provided a broad dynamic range (7 orders of magnitude) and a low LOD of 0.3 pM, leading to accurate SARS-CoV-2 antibody quantification (sensitivity/specificity of 100%/99%, with a portable optical fiber device).[208] Reverse transcription-quantitative polymerase chain reaction (RT-qPCR) was successfully performed in a reaction vessel containing PCR chemistry, fluorescent probes, and plasmonic nanoparticles using plasmonic thermocycling, in which rapid heating of the solution was achieved via infrared excitation of gold nanorods.[209] The authors achieved SARS-CoV-2 RNA detection in human saliva and nasal specimens with 100% sensitivity and 100% specificity.[209] Lew et al. have demonstrated a colorimetric serological assay to detect SARS-CoV-2 IgGs in patients' plasma using short antigenic epitopes conjugated to 13 nm AuNPs.[210] By testing 35 clinical plasma samples of varying illness severity, the authors were able to identify SARS-CoV-2 infection with 100% specificity and 83% sensitivity.[210]

The detection of spike proteins of alpha, beta, and gamma variants of the COVID-19 virus was achieved by specific nanostructured molecularly imprinted polymers (nanoMIPs).[211] The nanoMIP-functionalised LSPR sensor detected all 3 protein variants with a limit of detection of 9.71 fM, 7.32 fM and 8.81 pM using wavelength shifts for alpha, beta and gamma spike protein variants, respectively.[211] The LSPR sensing scheme of this device is based on Ag nanoparticles with an average diameter of 22.47 nm and an aspect ratio of 1.15 on a glass substrate.[211] A three-dimensional porous microplasma-engineered nanoassembly (AgMEN) was fabricated to provide a high sensitivity to SARS-CoV-2 S variants, including wild-type, alpha, delta, and omicron detection via remarkable SERS signal collection.[212] An LOD of 1 fg mL^{-1} and 0.1 pg mL^{-1} was noted for the S and N spike proteins, respectively.[212]

Behrouzi and Lin applied LSPR of antigen-coated AuNPs to detect the N protein of SARS-CoV-2.[137] This detection method gave naked-eye results in 5 min and an LOD of 150 ng mL^{-1}.[137] Park et al. used self-assembled AuNP arrays for the detection of the SARS-CoV-2 S protein.[213] Their biosensor gave quick results with high sensitivity in just 10 min and without any purification steps.[213] Both aforementioned sensors could be used for the PoC detection of SARS-CoV-2. In addition, Das et al. achieved an LOD of the S protein of 111.11 deg RIU^{-1} using a gold nanorod with a Kretschmann prism configuration.[214] Zavyalov et al. built a SERS aptasensor based on hydroxylamine-reduced AgNP substrates and successfully detected SARS-CoV-2 in about 7 min with an

LOD of 5.5×10^4 median tissue culture infectious dose per mL.[215] Tripathi et al. deposited AgNPs over glass coverslips and used them as SERS substrates.[216] The sensor was used to detect the Japanese encephalitis virus and demonstrated ultrasensitive detection, with a detection limit of 7.6 ng mL^{-1} and a linear response from 5 to 80 ng mL^{-1}.[216] A colorimetric assay based on AgNPs with diameters less than 60 nm and capped with thiol-modified antisense oligonucleotides specific for the N protein of SARS-CoV-2 has been demonstrated as being capable of diagnosing positive COVID-19 cases from isolated RNA samples within approximately 10 min.[217] A naked-eye (equipment-free), label-free, and RNA extraction-free method for SARS-CoV-2 detection was developed by employing anisotropic Au nanoparticles.[218] In this study, a specific sequence in the N-gene of SARS-CoV-2 was selected as a target to design antisense oligonucleotides (ASOs) with an extra strand polyguanine (G12).[218] Inactivated virus samples were added to anisotropic AuNPs synthesized on four ASOs, and after the annealing process, the color of the solution changed from red to purple.[218] The authors noted that in microfluidic paper-based analytical devices, this conjugation method allowed hybridization and annealing without a denaturation step, and its corresponding color change could be observed by the naked eye in the detection zone.[218]

4 Perspectives and outlook

Progress in material science and fundamental optics will continue to provide advantages to biosensing research. An important facilitator of this progress is the use of numerical analysis tools, such as COMSOL Multiphysics software,[38] to explore geometrical and material parameters for the optimization of the biosensor's performance. The combination of various optical and non-optical, for example electrochemical, detection configurations on a single platform could also enable multifunctional biosensors to extract information from a given sample. For example, plasmon-enhanced electrochemiluminescence (ECL)-based sensors are a promising option that deserves further attention.[219] The ECL process uses an oxidized luminescent substrate to stimulate a fluorescent acceptor.[219] Therefore, non-specific signals that are caused by external light can be minimized. In this regard, Fan et al. developed an ECL-based biosensor that amplifies the signal by employing a DNA walker strategy for the detection of the SARS CoV-2 RdRp gene.[220] Despite their simplicity and high sensitivity, plasmon-enhanced ECL-based biosensors present many challenges when used in point of care tests;[220] more efforts are needed to overcome them. In light of this, plasmonic colorimetric biosensing based on etching or growth of metal nanomaterials presents excellent prospects due to their simplicity and ease of use as test strips.[221] In order to detect SARS-CoV-2, colorimetric tests were developed using plasmonic biosensors with Au nanoparticles functionalized with polyclonal antibodies (f-AuNPs).[222] The authors observed

intense color changes with the naked eye when f-AuNPs accumulated on the virus and noted a detection limit of 0.28 PFU mL^{-1} in human saliva.[222] In addition, the integration of SERS with etching-based plasmonic colorimetric sensors could lead to novel, extremely sensitive detection devices.[221] Thus, it is possible to significantly improve detection accuracy and reproducibility, as well as detect targets in complex samples and serum, by combining several detection methods.

Likewise, two-dimensional materials, such as graphene, can provide dynamic control of plasmonic resonances, which is needed for small molecule detection.[223] Moreover, we envision that hybrid substrate integrating polar materials, van der Waals heterostructures, metal antennas, and metasurfaces will open new avenues for future biosensing innovation. Furthermore, integration with birefringent and chiral metamaterials for example chiral plasmon[224] layers for measuring chiro-optic response could advance enantioselective biochemical sensing applications.

Another alternative technique to be considered is nanopore technology, which allows for the precise detection of subunits as well as the sequencing of pathogen DNA and RNA in an effective and versatile way; this technology will be at the forefront of future state-of-the-art approaches.[225] Nanopore-based sequencing systems, such as the one developed by Oxford Nanopore Technologies, were successfully applied to SARS-CoV-2 strains at the early stages of the pandemic.[226,227] The rapid and real-time detection of mutagenized virus is a key benefit of this technique, providing important data for further epidemiological analysis.

In parallel, the availability of a variety of metal nanoparticle synthesis protocols, as well as an increase in the number of commercial nanoparticle providers, may contribute to the development of novel biosensors with high specificity and selectivity.[1,5,43,144] To develop high-sensitivity tests for SARS-CoV-2, the selection of metallic nanoparticles with appropriate sizes and shapes is a key point since their physical and optical properties can greatly influence the performance of a nanoparticle-based diagnostic system. Although spherical nanoparticles have been studied most extensively because of their ease of synthesis, other shapes are worth investigating when a higher sensitivity or a different sensing strategy is desired but not achievable with nanospheres. Regarding nanoparticle size, large metallic nanoparticles have large absorption cross-sections and may result in systems with higher sensitivities than those utilizing small nanoparticles. However, all of these parameters need to be addressed and evaluated on a project-by-project basis as many other factors could influence the LOD.[228]

Despite the excellent biosensing performance of plasmonic diagnostic tools, several technological aspects still require considerable improvement before fully operative devices for clinical diagnosis and real-world applications can be realized. Factors that need to be addressed include cost, sensitivity, specificity, and reproducibility, as well as user

interfaces and connectivity that allow for real-time monitoring of data collection. In terms of cost, inexpensive disposal chips are necessary to avoid cross-contamination issues and complicated cleaning procedures while handling biological samples or body fluids. In this regard, an integrated approach that allows for single-use cartridges and a stand-alone reader is desirable. Microfluidic technology can also play a key role in providing disposable, stable over time, and easy to manipulate cartridges through the incorporation of biochips with specific biofunctionalities for each detection assay. For airborne respiratory viruses, it will be essential to integrate such cartridges with additional safety steps, including sample preprocessing, before final detection.[229] Another possible advancement is the merging of plasmonic devices with smartphones; their light sources, cameras, and image processing and communication capabilities can reduce costs and facilitate large scale distribution.[230–233] Therefore, the development of portable and wireless nanobiosensors is essential for diverse applications. Sample collection and processing is an additional consideration for on-site biosensing. The large diversity of analytes and the matrix composition of specimens such as body fluids still remain a challenge. For example, virus detection from clinical specimens is still limited owing to the lack of suitable methods to prevent the interference of biomolecules in body fluids. In this sense, the design of antifouling coatings that can take into account either the composition of the media or the biological receptor's characteristics may help to bridge the gap between common analytical methods and plasmonic biosensing applications.

In summary, this tutorial review highlighted the physics underpinning the mechanics of plasmonic-based biosensors, the current progress of biosensor research, and the ability of such devices to detect virus particles viruses. It is worth noting that, although high sensitivity is always the main goal of any biosensor, for better clinical and commercial translation, it is essential to balance the trade-off between the sensitivity, cost-effectiveness, portability, and stability of these plasmonic-based systems. Against the backdrop of the COVID-19 global pandemic, continued biosensor development is crucial for the realization of more portable and affordable platforms that can meet global healthcare needs.

Conflicts of interest

The authors declare that they don't have any competing financial interests or personal relationships that could have appeared to influence the work reported in this tutorial review.

Acknowledgements

Notes and references

1 M. Soler, M. C. Estevez, M. Cardenosa-Rubio, A. Astua and L. M. Lechuga, *ACS Sens.*, 2020, **5**, 2663–2678.

2 G. Giovannini, H. Haick and D. Garoli, *ACS Sens.*, 2021, **6**, 1408–1417.

3 M. M. Hassan, F. S. Sium, F. Islam and S. M. Choudhury, *Sens. Bio-Sens. Res.*, 2021, **33**, 100429.

4 A. Asghari, C. Wang, K. M. Yoo, A. Rostamian, X. Xu, J.-D. Shin, H. Dalir and R. T. Chen, *Appl. Phys. Rev.*, 2021, **8**, 031313.

5 H. Altug, S.-H. Oh, S. A. Maier and J. Homola, *Nat. Nanotechnol.*, 2022, **17**, 5–16.

6 A. A. Serafetinides, M. Makropoulou, D. G. Kotsifaki and G. Tsigaridas, *Society of Photo-Optical Instrumentation Engineers (SPIE) Conference Series*, 2016, p. 1022613.

7 A. M. Caliendo, *Clin. Infect. Dis.*, 2011, **52**, S326–S330.

8 N. Boonham, J. Kreuze, S. Winter, R. van der Vlugt, J. Bergervoet, J. Tomlinson and R. Mumford, *Virus Res.*, 2014, **186**, 20–31.

9 V. M. Corman, O. Landt, M. Kaiser, R. Molenkamp, A. Meijer, D. K. Chu, T. Bleicker, S. Brünink, J. Schneider, M. L. Schmidt, D. G. Mulders, B. L. Haagmans, B. van der Veer, S. van den Brink, L. Wijsman, G. Goderski, J.-L. Romette, J. Ellis, M. Zambon, M. Peiris, H. Goossens, C. Reusken, M. P. Koopmans and C. Drosten, *Eurosurveillance*, 2020, **25**, 1–8.

10 F. Cui and H. S. Zhou, *Biosens. Bioelectron.*, 2020, **165**, 112349.

11 J. Louten, *Essential Human Virology*, Academic Press, Boston, 2016, pp. 19–29.

12 C. M. Michaud, *Encyclopedia of Microbiology (Third Edition)*, Academic Press, Oxford, 3rd edn, 2009, pp. 444–454.

13 R. Funari, K.-Y. Chu and A. Q. Shen, *Biosens. Bioelectron.*, 2020, **169**, 112578.

14 L. Rubio, L. Galipienso and I. Ferriol, *Front. Plant Sci.*, 2020, **11**, 1092.

15 C. J. Menendez-Botet, *Clin. Chem.*, 2003, **49**, 1424–1425.

16 D. Mabey, R. W. Peeling, A. Ustianowski and M. D. Perkins, *Nat. Rev. Microbiol.*, 2004, **2**, 231–240.

17 A. K. Yetisen, M. S. Akram and C. R. Lowe, *Lab Chip*, 2013, **13**, 2210–2251.

18 X. A. Zhang, I.-T. Chen and C.-H. Chang, *Nanotechnology*, 2019, **30**, 352002.

19 P. L. Mage, B. S. Ferguson, D. Maliniak, K. L. Ploense, T. E. Kippin and H. T. Soh, *Nat. Biomed. Eng.*, 2017, **1**, 0070.

20 E. W. A. Visser, J. Yan, L. J. van Ijzendoorn and M. W. Prins, *Nat. Commun.*, 2018, **9**, 2541.

21 J. Heikenfeld, A. YJajack, B. Feldman, S. W. Granger, S. Gaitonde, G. Begtrup and B. A. Katchman, *Nat. Biotechnol.*, 2019, **37**, 407–419.

22 M. U. Ahmed, I. Saaem, P. C. Wu and A. S. Brown, *Crit. Rev. Biotechnol.*, 2014, **34**, 180–196.

23 D. Ho, S. R. Quake, E. R. McCabe, W. J. Chng, E. K. Chow, X. Ding, B. D. Gelb, G. S. Ginsburg, J. Hassenstab, C.-M. Ho, W. C. Mobley, G. P. Nolan, S. T. Rosen, P. Tan, Y. Yen and A. Zarrinpar, *Trends Biotechnol.*, 2020, **38**, 497–518.

24 S. Roh, T. Chung and B. Lee, *Sensors*, 2011, **11**, 1565–1588.

25 J. Wang, A. J. Drelich, C. M. Hopkins, S. Mecozzi, L. Li, G. Kwon and S. Hong, *Wiley Interdiscip. Rev.: Nanomed. Nanobiotechnol.*, 2022, **14**, e1754.

26 S. J. Park, S. H. Cha, G. A. Shin and Y. H. Ahn, *Biomed. Opt. Express*, 2017, **8**, 3551–3558.

27 Z. Li, L. Leustean, F. Inci, M. Zheng, U. Demirci and S. Wang, *Biotechnol. Adv.*, 2019, **37**, 107440.

28 J. Lee, K. Takemura and E. Y. Park, *Sensors*, 2017, **17**, 2332.

29 D. G. Kotsifaki and S. Nic Chormaic, *Nanophotonics*, 2019, **8**, 1227–1245.

30 J.-H. Qu, A. Dillen, W. Saeys, J. Lammertyn and D. Spasic, *Anal. Chim. Acta*, 2020, **1104**, 10–27.

31 C. M. Das, Y. Guo, L. Kang, H.-p. Ho and K.-T. Yong, *Adv. Theory Simul.*, 2020, **3**, 2000074.

32 E. Mauriz, *Sensors*, 2020, **20**, 4745.

33 D. G. Kotsifaki and S. Nic Chormaic, *Nanophotonics*, 2022, **11**, 2199–2218.

34 L. Krejcova, L. Nejdl, M. A. M. Rodrigo, M. Zurek, M. Matousek, D. Hynek, O. Zitka, P. Kopel and V. Adam, *Biosens. Bioelectron.*, 2014, **54**, 421–427.

35 O. Adegoke, T. Kato and E. Y. Park, *Biosens. Bioelectron.*, 2016, **80**, 483–490.

36 L. La Spada and L. Vegni, *Materials*, 2018, **11**, 603.

37 Y. Pang, J. Jian, T. Tu, Z. Yang, J. Ling, Y. Li, X. Wang, Y. Qiao, H. Tian, Y. Yang and T.-L. Ren, *Biosens. Bioelectron.*, 2018, **116**, 123–129.

38 D. G. Kotsifaki, M. Makropoulou and A. A. Searfetinides, *Eur. Phys. J.: Appl. Phys.*, 2019, **86**, 30501.

39 R. Abdel-Karim, Y. Reda and A. Abdel-Fattah, *J. Electrochem. Soc.*, 2020, **167**, 037554.

40 J. Burkhartsmeyer, Y. Wang, K. S. Wong and R. Gordon, *Appl. Sci.*, 2020, **10**, 394.

41 V. Yesudasu, H. S. Pradhan and R. J. Pandya, *Heliyon*, 2021, **7**, e06321.

42 A. Abbas, M. J. Linman and Q. Cheng, *Biosens. Bioelectron.*, 2011, **26**, 1815–1824.

43 Y. Li, K. Zhao, H. Sobhani, K. Bao and P. Nordlander, *J. Phys. Chem. Lett.*, 2013, **4**, 1352–1357.

44 M. Couture, S. S. Zhao and J.-F. Masson, *Phys. Chem. Chem. Phys.*, 2013, **15**, 11190–11216.

45 H. Guner, E. Ozgur, G. Kokturk, M. Celik, E. Esen, A. E. Topal, S. Ayas, Y. Uludag, C. Elbuken and A. Dana, *Sens. Actuators, B*, 2017, **239**, 571–577.

46 L. Novotny and B. Hecht, *Principles of Nano-Optics*, Cambridge University Press, 2nd edn, 2012.

47 R. Wood, *Philos. Mag.*, 1902, **4**, 396–402.

48 L. Rayleigh, *Philos. Mag.*, 1907, **13**, 214–232.

49 R. H. Ritchie, *Phys. Rev.*, 1957, **106**, 874–881.

50 C. J. Powell and J. B. Swan, *Phys. Rev.*, 1960, **118**, 640–643.

51 A. Otto, *Z. Phys.*, 1968, **216**, 398–410.

52 E. Kretschmann and H. Raether, *Z. Naturforsch., A: Astrophys., Phys. Phys. Chem.*, 1968, **23**, 2135–2136.

53 T. D. Bouloumis and S. Nic Chormaic, *Appl. Sci.*, 2020, **10**, 1375.

54 M. Fleischmann, P. Hendra and A. McQuillan, *Chem. Phys. Lett.*, 1974, **26**, 163–166.

55 D. L. Jeanmaire and R. P. Van Duyne, *J. Electroanal. Chem. Interfacial Electrochem.*, 1977, **84**, 1–20.

56 B. Liedberg, C. Nylander and I. Lunström, *Sens. Actuators*, 1983, **4**, 299–304.

57 S. Scarano, M. Mascini, A. P. Turner and M. Minunni, *Biosens. Bioelectron.*, 2010, **25**, 957–966.

58 S. Mohammadzadeh-Asl, A. Keshtkar, J. Ezzati Nazhad Dolatabadi and M. de la Guardia, *Biosens. Bioelectron.*, 2018, **110**, 118–131.

59 M. Bocková, J. Slabý, T. Špringer and J. Homola, *Annu. Rev. Anal. Chem.*, 2019, **12**, 151–176.

60 K. A. Willets and R. P. Van Duyne, *Annu. Rev. Phys. Chem.*, 2007, **58**, 267–297.

61 P. B. Johnson and R. W. Christy, *Phys. Rev. B: Solid State*, 1972, **6**, 4370–4379.

62 H. U. Yang, J. D'Archangel, M. L. Sundheimer, E. Tucker, G. D. Boreman and M. B. Raschke, *Phys. Rev. B: Condens. Matter Mater. Phys.*, 2015, **91**, 235137.

63 N. J. Halas, S. Lal, W.-S. Chang, S. Link and P. Nordlander, *Chem. Rev.*, 2011, **111**, 3913–3961.

64 H. Raether, in *Surface plasmons on smooth surfaces*, Springer Berlin Heidelberg, Berlin, Heidelberg, 1988, pp. 4–39.

65 M. Li, S. K. Cushing and N. Wu, *Analyst*, 2015, **140**, 386–406.

66 C. M. Miyazaki, F. M. Shimizu and M. Ferreira, *Nanocharacterization Techniques*, William Andrew Publishing, 2017, pp. 183–200.

67 V. G. Kravets, A. V. Kabashin, W. L. Barnes and A. N. Grigorenko, *Chem. Rev.*, 2018, **118**, 5912–5951.

68 F. Ian, M. Nigel, S. Margaret and H. Catherine, *Gold Bull.*, 2008, **40**, 270–277.

69 P. Chen, M. T. Chung, W. McHugh, R. Nidetz, Y. Li, J. Fu, T. T. Cornell, T. P. Shanley and K. Kurabayashi, *ACS Nano*, 2015, **9**, 4173–4181.

70 A. G. Brolo, *Nat. Photonics*, 2012, **6**, 709–713.

71 S. S. Aćimović, M. A. Ortega, V. Sanz, J. Berthelot, J. L. Garcia-Cordero, J. Renger, S. J. Maerkl, M. P. Kreuzer and R. Quidant, *Nano Lett.*, 2014, **14**, 2636–2641.

72 D. G. Kotsifaki, M. D. Mackenzie, G. Polydefki, A. K. Kar, M. Makropoulou and A. A. Serafetinides, *Opt. Eng.*, 2017, **56**, 124111.

73 M. Moskovits, *Rev. Mod. Phys.*, 1985, **57**, 783–826.

74 J. Kundu, F. Le, P. Nordlander and N. J. Halas, *Chem. Phys. Lett.*, 2008, **452**, 115–119.

75 S. Fayyaz, M. Tabatabaei, R. Hou and F. Lagugné-Labarthet, *J. Phys. Chem. C*, 2012, **116**, 11665–11670.

76 A. B. Taylor and P. Zijlstra, *ACS Sens.*, 2017, **2**, 1103–1122.

77 B. Luk'yanchuk, N. I. Zheludev, S. A. Maier, N. J. Halas, P. Nordlander, H. Giessen and T. C. Chong, *Nat. Mater.*, 2010, **9**, 707–715.

78 A. Ahmadivand, B. Gerislioglu, R. Ahuja and Y. Kumar Mishra, *Mater. Today*, 2020, **32**, 108–130.

79 D. G. Kotsifaki, V. G. Truong and S. Nic Chormaic, *Nano Lett.*, 2020, **20**, 3388–3395.

80 D. G. Kotsifaki, V. G. Truong and S. Nic Chormaic, *Appl. Phys. Lett.*, 2021, **118**, 021107.

81 V. G. Veselago, *Sov. Phys. Usp.*, 1968, **10**, 509–514.

82 J. Pendry, A. Holden, D. Robbins and W. Stewart, *IEEE Trans. Microwave Theory Tech.*, 1999, **47**, 2075–2084.

83 D. R. Smith, W. J. Padilla, D. C. Vier, S. C. Nemat-Nasser and S. Schultz, *Phys. Rev. Lett.*, 2000, **84**, 4184–4187.

84 J. B. Pendry, *Phys. Rev. Lett.*, 2000, **85**, 3966–3969.

85 Y. Fang, Y. Ge, C. Wang and H. Zhang, *Laser Photonics Rev.*, 2020, **14**, 1900098.

86 P. Yu, L. V. Besteiro, Y. Huang, J. Wu, L. Fu, H. H. Tan, C. Jagadish, G. P. Wiederrecht, A. O. Govorov and Z. Wang, *Adv. Opt. Mater.*, 2019, **7**, 1800995.

87 M. Beruete and I. Jáuregui-López, *Adv. Opt. Mater.*, 2020, **8**, 1900721.

88 Y. Roh, S.-H. Lee, J. Kwak, H. S. Song, S. Shin, Y. K. Kim, J. W. Wu, B.-K. Ju, B. Kang and M. Seo, *Sens. Actuators, B*, 2022, **352**, 130993.

89 R. Zhou, C. Wang, W. Xu and L. Xie, *Nanoscale*, 2019, **11**, 3445–3457.

90 W. Wang, M. Ramezani, A. I. Väkeväinen, P. Törmä, J. G. Rivas and T. W. Odom, *Mater. Today*, 2018, **21**, 303–314.

91 M. Fan, G. F. Andrade and A. G. Brolo, *Anal. Chim. Acta*, 2020, **1097**, 1–29.

92 H. Shi, X. Zhu, S. Zhang, G. Wen, M. Zheng and H. Duan, *Nanoscale Adv.*, 2021, **3**, 4349–4369.

93 K. C. Bantz, A. F. Meyer, N. J. Wittenberg, H. Im, Ö. Kurtuluș, S. H. Lee, N. C. Lindquist, S.-H. Oh and C. L. Haynes, *Phys. Chem. Chem. Phys.*, 2011, **13**, 11551–11567.

94 E. C. Le Ru, E. Blackie, M. Meyer and P. G. Etchegoin, *J. Phys. Chem. C*, 2007, **111**, 13794–13803.

95 C. E. Anderson, C. A. Holstein, E.-M. Strauch, S. Bennett, A. Chevalier, J. Nelson, E. Fu, D. Baker and P. Yager, *Anal. Chem.*, 2017, **89**, 6608–6615.

96 T. J. Moore, A. S. Moody, T. D. Payne, G. M. Sarabia, A. R. Daniel and B. Sharma, *Biosensors*, 2018, **8**, 46.

97 G. Spoto and M. Minunni, *J. Phys. Chem. Lett.*, 2012, **3**, 2682–2691.

98 Y. Zeng, R. Hu, L. Wang, D. Gu, J. He, S.-Y. Wu, H.-P. Ho, X. Li, J. Qu, B. Z. Gao and Y. Shao, *Nanophotonics*, 2017, **6**, 1017–1030.

99 Z. Huo, Y. Li, B. Chen, W. Zhang, X. Yang and X. Yang, *Talanta*, 2023, **255**, 124213.

100 J.-S. Lin, X.-D. Tian, G. Li, F.-L. Zhang, Y. Wang and J.-F. Li, *Chem. Soc. Rev.*, 2022, **51**, 9445–9468.

101 E. A. Smith and R. M. Corn, *Appl. Spectrosc.*, 2003, **57**, 320A–332A.

102 D. Kotsifaki and A. Serafetinides, *Opt. Laser Technol.*, 2011, **43**, 1448–1452.

103 D. Kotsifaki and A. Serafetinides, *Opt. Laser Technol.*, 2009, **41**, 365–373.

104 D. G. Kotsifaki, M. Makropoulou and A. A. Serafetinides, *16th International School on Quantum Electronics: Laser Physics and Applications*, 2011, p. 77470Z.

105 D. G. Kotsifaki, S. Aggelopoulos, M. Makropoulou and A. Serafetinides, *J. Nanotechnol. Diagn. Treat.*, 2016, **4**, 25–30.

106 C. Christophe, G. Tuan and A. Jacques, *Anal. Bioanal. Chem.*, 2015, **407**, 3883–3897.

107 Q. Wang and L. Wang, *Nanoscale*, 2020, **12**, 7485–7499.

108 Y. Esfahani Monfared, *Biosensors*, 2020, **10**, 77.

109 Z. Wang, W. Zhang, X. Liu, M. Li, X. Lang, R. Singh, C. Marques, B. Zhang and S. Kumar, *Biosensors*, 2022, **12**, 1016.

110 P. Estrela, N. Bhalla, P. Jolly, N. Formisano and P. Estrela, *Essays Biochem.*, 2016, **60**, 1–8.

111 Y. Huang, J. Xu, J. Liu, X. Wang and B. Chen, *Sensors*, 2017, **17**, 2375.

112 A. N. Kozitsina, T. S. Svalova, N. N. Malysheva, A. V. Okhokhonin, M. B. Vidrevich and K. Z. Brainina, *Biosensors*, 2018, **8**, 35.

113 B. Špačková, P. Wrobel, M. Bocková and J. Homola, *Proc. IEEE*, 2016, **104**, 2380–2408.

114 M. M. Miller and A. A. Lazarides, *J. Phys. Chem. B*, 2005, **109**, 21556–21565.

115 A. A. Kolomenskii, P. D. Gershon and H. A. Schuessler, *Appl. Opt.*, 1997, **36**, 6539–6547.

116 L. S. Live, O. R. Bolduc and J.-F. Masson, *Anal. Chem.*, 2010, **82**, 3780–3787.

117 M. Piliarik and J. Homola, *Opt. Express*, 2009, **17**, 16505–16517.

118 D. J. Bergman and M. I. Stockman, *Phys. Rev. Lett.*, 2003, **90**, 027402.

119 A. A. Yanik, A. E. Cetin, M. Huang, A. Artar, S. H. Mousavi, A. Khanikaev, J. H. Connor, G. Shvets and H. Altug, *Proc. Natl. Acad. Sci. U. S. A.*, 2011, **108**, 11784–11789.

120 S. Zhang, K. Bao, N. J. Halas, H. Xu and P. Nordlander, *Nano Lett.*, 2011, **11**, 1657–1663.

121 P. Offermans, M. C. Schaafsma, S. R. K. Rodriguez, Y. Zhang, M. Crego-Calama, S. H. Brongersma and J. Gómez Rivas, *ACS Nano*, 2011, **5**, 5151–5157.

122 Y.-F. Chang, W.-H. Wang, Y.-W. Hong, R.-Y. Yuan, K.-H. Chen, Y.-W. Huang, P.-L. Lu, Y.-H. Chen, Y.-M. A. Chen, L.-C. Su and S.-F. Wang, *Anal. Chem.*, 2018, **90**, 1861–1869.

123 B. A. Prabowo, R. Y. Wang, M. K. Secario, P.-T. Ou, A. Alom, J.-J. Liu and K.-C. Liu, *Biosens. Bioelectron.*, 2017, **92**, 186–191.

124 L. Shi, Q. Sun, J. He, H. Xu, C. Liu, C. Zhao, Y. Xu, C. Wu, J. Xiang, D. Gu, J. Long and H. Lan, *Bio-Med. Mater. Eng.*, 2015, **26**, S2207–S2216.

125 S. K. Pushpendra, K. S. Jyoti, S. V. Virendra, B. Utpal, S. S. Shyam, A. I. Syed, D. K. Paban, B. Mannan, G. Kumaran and J. Rajeev, *Anal. Bioanal. Chem.*, 2020, **412**, 4101–41120.

126 W. Diao, M. Tang, S. Ding, X. Li, W. Cheng, F. Mo, X. Yan, H. Ma and Y. Yan, *Biosens. Bioelectron.*, 2018, **100**, 228–234.

127 M. Rippa, R. Castagna, S. Brandi, G. Fusco, M. Monini, D. Chen, J. Zhou, J. Zyss and L. Petti, *ACS Appl. Nano Mater.*, 2020, **3**, 4837–4844.

128 A. Ahmadivand, B. Gerislioglu, A. Tomitaka, P. Manickam, A. Kaushik, S. Bhansali, M. Nair and N. Pala, *Biomed. Opt. Express*, 2018, **9**, 373–386.

129   A. Ahmadivand, B. Gerislioglu, Z. Ramezani, A. Kaushik, P. Manickam and S. A. Ghoreishi, *Biosens. Bioelectron.*, 2021, **177**, 112971.

130   G. Qiu, Z. Gai, Y. Tao, J. Schmitt, G. A. Kullak-Ublick and J. Wang, *ACS Nano*, 2020, **14**, 5268–5277.

131   J. Kim, S. Y. Oh, S. Shukla, S. B. Hong, N. S. Heo, V. Bajpai, H. S. Chun, C.-H. Jo, B. G. Choi, Y. S. Huh and Y.-K. Han, *Biosens. Bioelectron.*, 2018, **107**, 118–122.

132   T. Lee, G. H. Kim, S. M. Kim, K. Hong, Y. Kim, C. Park, H. Sohn and J. Min, *Colloids Surf., B*, 2019, **182**, 110341.

133   N. S. Heo, S. Y. Oh, M. Y. Ryu, S. H. Baek, T. J. Park, C. Choi, Y. S. Huh and J. P. Park, *Biotechnol. Bioprocess Eng.*, 2019, **24**, 318–325.

134   A. M. Paul, Z. Fan, S. S. Sinha, Y. Shi, L. Le, F. Bai and P. C. Ray, *J. Phys. Chem. C*, 2015, **119**, 23669–23675.

135   S. A. Camacho, R. G. Sobral-Filho, P. H. B. Aoki, C. J. L. Constantino and A. G. Brolo, *ACS Sens.*, 2018, **3**, 587–594.

136   P. P. Austin Suthanthiraraj and A. K. Sen, *Biosens. Bioelectron.*, 2019, **132**, 38–46.

137   K. Behrouzi and L. Lin, *Biosens. Bioelectron.*, 2022, **195**, 113669.

138   E. Wijaya, C. Lenaerts, S. Maricot, J. Hastanin, S. Habraken, J.-P. Vilcot, R. Boukherroub and S. Szunerits, *Curr. Opin. Solid State Mater. Sci.*, 2011, **15**, 208–224.

139   J. Liu, M. Jalali, S. Mahshid and S. Wachsmann-Hogiu, *Analyst*, 2020, **145**, 364–384.

140   T. Liyanage, B. Alharbi, L. Quan, A. Esquela-Kerscher and G. Slaughter, *ACS Omega*, 2022, **7**, 2411–2418.

141   G. Nava, G. Zanchetta, F. Giavazzi and M. Buscaglia, *Nanophotonics*, 2022, **11**, 4159–4181.

142   D. Kotsifaki, M. Makropoulou and A. A. Serafetinides, *Saratov Fall Meeting 2006: Optical Technologies in Biophysics and Medicine VIII*, 2007, p. 65351O.

143   J. Homola, *Chem. Rev.*, 2008, **108**, 462–493.

144   J. Wang, A. J. Drelich, C. M. Hopkins, S. Mecozzi, L. Li, G. Kwon and S. Hong, *Wiley Interdiscip. Rev.: Nanomed. Nanobiotechnol.*, 2022, **14**, e1754.

145   D. Schofield and N. Dimmock, *J. Virol. Methods*, 1996, **62**, 33–42.

146   Ravina, A. Dalal, H. Mohan, M. Prasad and C. Pundir, *Biosci. Rep.*, 2020, **40**, 1–18.

147   F. Zang, Z. Su, L. Zhou, K. Konduru, G. Kaplan and S. Y. Chou, *Adv. Mater.*, 2019, **31**, 1902331.

148   J. A. Jackman, E. Linardy, D. Yoo, J. Seo, W. B. Ng, D. J. Klemme, N. J. Wittenberg, S.-H. Oh and N.-J. Cho, *Small*, 2016, **12**, 1159–1166.

149   Z. Klestova, A. Voronina, A. Yushchenko, O. Vatlitsova, G. Dorozinsky, Y. Ushenin, V. Maslov, T. Doroshenko and S. Kravchenko, *Spectrochim. Acta, Part A*, 2022, **264**, 120236.

150   H.-Y. Hsieh, R. Chang, Y.-Y. Huang, P.-H. Juan, H. Tahara, K.-Y. Lee, D. N. K. Vo, M.-H. Tsai, P.-K. Wei, H.-J. Sheen and Y.-J. Fan, *Biosens. Bioelectron.*, 2022, **195**, 113672.

151   H. A. Bethe, *Phys. Rev.*, 1944, **66**, 163–182.

152   A. A. Yanik, M. Huang, O. Kamohara, A. Artar, T. W. Geisbert, J. H. Connor and H. Altug, *Nano Lett.*, 2010, **10**, 4962–4969.

153   G. Qiu, Z. Gai, L. Saleh, J. Tang, T. Gui, G. A. Kullak-Ublick and J. Wang, *ACS Nano*, 2021, **15**, 7536–7546.

154   N. Cennamo, L. Pasquardini, F. Arcadio, L. Lunelli, L. Vanzetti, V. Carafa, L. Altucci and L. Zeni, *Talanta*, 2021, **233**, 122532.

155   N. Cennamo, G. D'Agostino, C. Perri, F. Arcadio, G. Chiaretti, E. M. Parisio, G. Camarlinghi, C. Vettori, F. Di Marzo, R. Cennamo, G. Porto and L. Zeni, *Sensors*, 2021, **21**, 1681.

156   L. Yu, L. Hao, T. Meiqiong, H. Jiaoqi, L. Wei, D. Jinying, C. Xueping, F. Weiling and Z. Yang, *RSC Adv.*, 2019, **9**, 9354–9363.

157   L. Huang, L. Ding, J. Zhou, S. Chen, F. Chen, C. Zhao, J. Xu, W. Hu, J. Ji, H. Xu and G. L. Liu, *Biosens. Bioelectron.*, 2021, **171**, 112685.

158   M. Forinová, A. Pilipenco, I. Víšová, N. S. J. Lynn, J. Dostálek, H. Mašková, V. Hönig, M. Palus, M. Selinger, P. Kočová, F. Dyčka, J. Štěrba, M. Houska, M. Vrabcová, P. Horák, J. Anthi, C.-P. Tung, C.-M. Yu, C.-Y. Chen, Y.-C. Huang, P.-H. Tsai, S.-Y. Lin, H.-J. Hsu, A.-S. Yang, A. Dejneka and H. Vaisocherová-Lísalová, *ACS Appl. Mater. Interfaces*, 2021, **13**, 60612–60624.

159   B. Yin, W. K. H. Ho, Q. Zhang, C. Li, Y. Huang, J. Yan, H. Yang, J. Hao, S. H. D. Wong and M. Yang, *ACS Appl. Mater. Interfaces*, 2022, **14**, 4714–4724.

160   O. Calvo-Lozano, M. Sierra, M. Soler, M. C. Estévez, L. Chiscano-Camón, A. Ruiz-Sanmartin, J. C. Ruiz-Rodriguez, R. Ferrer, J. J. González-López, J. Esperalba, C. Fernández-Naval, L. Bueno, R. López-Aladid, A. Torres, L. Fernández-Barat, S. Attoumani, R. Charrel, B. Coutard and L. M. Lechuga, *Anal. Chem.*, 2022, **94**, 975–984.

161   I. B. Ansah, S. H. Lee, J.-Y. Yang, C. Mun, S. Jung, H. S. Jung, M.-Y. Lee, T. Kang, S. Lee, D.-H. Kim and S.-G. Park, *Biosens. Bioelectron.*, 2023, **220**, 114930.

162   G. Palermo, M. Rippa, Y. Conti, A. Vestri, R. Castagna, G. Fusco, E. Suffredini, J. Zhou, J. Zyss, A. De Luca and L. Petti, *ACS Appl. Mater. Interfaces*, 2021, **13**, 43715–43725.

163   K. S. Novoselov, A. K. Geim, S. V. Morozov, D. Jiang, Y. Zhang, S. V. Dubonos, I. V. Grigorieva and A. A. Firsov, *Science*, 2004, **306**, 666–669.

164   C. Ménard-Moyon, A. Bianco and K. Kalantar-Zadeh, *ACS Sens.*, 2020, **5**, 3739–3769.

165   N. Rohaizad, C. C. Mayorga-Martinez, M. Fojtů, N. M. Latiff and M. Pumera, *Chem. Soc. Rev.*, 2021, **50**, 619–657.

166   M. M. Y. A. Alsaif, K. Latham, M. R. Field, D. D. Yao, N. V. Medehkar, G. A. Beane, R. B. Kaner, S. P. Russo, J. Z. Ou and K. Kalantar-zadeh, *Adv. Mater.*, 2014, **26**, 3931–3937.

167   B. Y. Zhang, A. Zavabeti, A. F. Chrimes, F. Haque, L. A. O'Dell, H. Khan, N. Syed, R. Datta, Y. Wang, A. S. R. Chesman, T. Daeneke, K. Kalantar-zadeh and J. Z. Ou, *Adv. Funct. Mater.*, 2018, **28**, 1706006.

168   T. Low, A. Chaves, J. D. Caldwell, A. Kumar, N. X. Fang, P. Avouris, T. F. Heinz, F. Guinea, L. Martin-Moreno and F. Koppens, *Nat. Mater.*, 2017, **16**, 182–194.

169 A. Bolotsky, D. Butler, C. Dong, K. Gerace, N. R. Glavin, C. Muratore, J. A. Robinson and A. Ebrahimi, *ACS Nano*, 2019, **13**, 9781–9810.

170 S.-H. Oh, H. Altug, X. Jin, S. J. K. Tony Low, A. P. Ivanov, J. B. Edel, P. Avouris and M. S. Strano, *Nat. Commun.*, 2021, **12**, 3824.

171 M.-Q. Fu, X.-C. Wang, W.-T. Dou, G.-R. Chen, T. D. James, D.-M. Zhou and X.-P. He, *Chem. Commun.*, 2020, **56**, 5735–5738.

172 N. A. S. Omar, Y. W. Fen, S. Saleviter, W. M. E. M. M. Daniyal, N. A. A. Anas, N. S. M. Ramdzan and M. D. A. Roshidi, *Materials*, 2019, **12**, 1928.

173 X. Peng, Y. Zhang, D. Lu, Y. Guo and S. Guo, *Sens. Actuators, B*, 2019, **286**, 222–229.

174 J. Z. Ou, A. F. Chrimes, Y. Wang, S.-y. Tang, M. S. Strano and K. Kalantar-zadeh, *Nano Lett.*, 2014, **14**, 857–863.

175 Y. Liu, Y. Nie, M. Wang, Q. Zhang and Q. Ma, *Biosens. Bioelectron.*, 2020, **148**, 111823.

176 S. Barua, H. S. Dutta, S. Gogoi, R. Devi and R. Khan, *ACS Appl. Nano Mater.*, 2018, **1**, 2–25.

177 V. Yadav, S. Roy, P. Singh, Z. Khan and A. Jaiswal, *Small*, 2019, **15**, 1803706.

178 T. B. A. Akib, S. F. Mou, M. M. Rahman, M. M. Rana, M. R. Islam, I. M. Mehedi, M. A. P. Mahmud and A. Z. Kouzani, *Sensors*, 2021, **21**, 3491.

179 S. Mostufa, T. B. A. Akib, M. M. Rana, I. M. Mehedi, U. M. Al-Saggaf, A. U. Alsaggaf, M. U. Alsaggaf and M. S. Alam, *Opt. Continuum*, 2022, **1**, 494–515.

180 N. H. L. Nguyen, S. Kim, G. Lindemann and V. Berry, *ACS Nano*, 2021, **15**, 11743–11752.

181 S. Addanki, I. Amiri and P. Yupapin, *Results Phys.*, 2018, **10**, 743–750.

182 A. G. Podoleanu, *J. Lightwave Technol.*, 2010, **28**, 624–640.

183 Y. Esfahani Monfared, *Biosensors*, 2020, **10**, 77.

184 G. Gauglitz, *Anal. Bioanal. Chem.*, 2020, **412**, 3317–3349.

185 X. Zhao, Y.-C. Tsao, F.-J. Lee, W.-H. Tsai, C.-H. Wang, T.-L. Chuang, M.-S. Wu and C.-W. Lin, *J. Virol. Methods*, 2016, **233**, 15–22.

186 H.-Y. Lin, C.-H. Huang, S.-H. Lu, I.-T. Kuo and L.-K. Chau, *Biosens. Bioelectron.*, 2014, **51**, 371–378.

187 B. Luo, Y. Xu, S. Wu, M. Zhao, P. Jiang, S. Shi, Z. Zhang, Y. Wang, L. Wang and Y. Liu, *Biosens. Bioelectron.*, 2018, **100**, 169–175.

188 D. Murugan, H. Bhatia, V. V. R. Sai and S. Jitendra, *Transactions of the Indian National Academy of Engineering*, 2020, **5**, 211–215.

189 M. Aliee and H. M. Mozaffari, *Plasmonics*, 2022, **17**, 1655–1660.

190 S. Yosra, H. G. Mohamed, M. Karine, S. Marwa and B. Hafedh, *Plasmonics*, 2022, **17**, 1489–1500.

191 L. Wu, H. S. Chu, W. S. Koh and E. P. Li, *Opt. Express*, 2010, **18**, 14395–14400.

192 A. Wei, M. Thomas, J. Mehtala and J. Wang, *Biomaterials for Cancer Therapeutics*, Woodhead Publishing, 2013, pp. 349–389.

193 N. Ibrahim, N. D. Jamaluddin, L. L. Tan and N. Y. Mohd Yusof, *Sensors*, 2021, **21**, 5114.

194 H. Geng, S. Vilms Pedersen, Y. Ma, T. Haghighi, H. Dai, P. D. Howes and M. M. Stevens, *Acc. Chem. Res.*, 2022, **55**, 593–604.

195 K. Takemura, O. Adegoke, T. Suzuki and E. Y. Park, *PLoS One*, 2019, **14**, e0211517.

196 A. D. Chowdhury, K. Takemura, I. M. Khorish, F. Nasrin, M. M. N. Tun, K. Morita and E. Y. Park, *Nanoscale Adv.*, 2020, **2**, 699–709.

197 J. Luan, A. Seth, R. Gupta, Z. Wang, P. Rathi, S. Cao, H. G. Derami, R. Tang, B. Xu, S. Achilefu, J. J. Morrissey and S. Singamanen, *Nat. Biomed. Eng.*, 2020, **4**, 518–530.

198 S. Das, D. K. Agarwal, B. Mandal, V. R. Rao and T. Kundu, *ACS Omega*, 2021, **6**, 17413–17423.

199 H. Liang, H. Wei, D. Pan and H. Xu, *Nanotechnol. Rev.*, 2015, **4**, 289–302.

200 T.-H. Kim, M. Kim, H.-S. Park, U. S. Shin, M.-S. Gong and H.-W. Kim, *J. Biomed. Mater. Res., Part A*, 2012, **100**, 1033–1043.

201 Q. Zhang, J. Hong and X. Y. Biofuels, *Methods Mol. Biol.*, 2012, **581**, 1–330.

202 S. S. Jeremiah, K. Miyakawa, T. Morita, Y. Yamaoka and A. Ryo, *Biochem. Biophys. Res. Commun.*, 2020, **533**, 195–200.

203 A. Salleh, R. Naomi, N. D. Utami, A. W. Mohammad, E. Mahmoudi, N. Mustafa and M. B. Fauzi, *Nanomaterials*, 2020, **10**, 1566.

204 Y. Wang, Y. Kang, W. Y. Wang, Q. Ding, J. Zhou and S. Yang, *Nanotechnology*, 2018, **29**, 414001.

205 M. Tejamaya, I. Römer, R. C. Merrifield and J. R. Lead, *Environ. Sci. Technol.*, 2012, **46**, 7011–7017.

206 J. Hong, S. Jun, S. Cha, J. Park, S. Lee, G. Shin and Y. Ahn, *Sci. Rep.*, 2018, **8**, 1–8.

207 Y. Lu, Y. Lin, Z. Zheng, X. Tang, J. Lin, X. Liu, M. Liu, G. Chen, S. Qiu, T. Zhou, Y. Lin and S. Feng, *Biomed. Opt. Express*, 2018, **9**, 4755–4766.

208 J. Nan, W. Sun, X. Liu, Y. Che, H. Shan, Y. Yue, J. Liu, L. Wang, K. Liu, W. Xu, W. Zhang, S. Zhang, B. Liu, K. S. Hettie, S. Zhu, J. Zhang and B. Yang, *Nano Lett.*, 2022, **22**, 9596–9605.

209 N. R. Blumenfeld, M. A. E. Bolene, M. Jaspan, A. G. Ayers, S. Zarrandikoetxea, J. Freudman, N. Shah, A. M. Tolwani, Y. Hu, T. L. Chern, J. Rogot, V. Behnam, A. Sekhar, X. Liu, B. Onalir, R. Kasumi, A. Sanogo, K. Human, K. Murakami, G. S. Totapally, M. Fasciano and S. K. Sia, *Nat. Nanotechnol.*, 2022, **17**, 984–992.

210 T. T. S. Lew, K. M. M. Aung, S. Y. Ow, S. N. Amrun, L. Sutarlie, L. F. P. Ng and X. Su, *ACS Nano*, 2021, **15**, 12286–12297.

211 N. Bhalla, A. F. Payam, A. Morelli, P. K. Sharma, R. Johnson, A. Thomson, P. Jolly and F. Canfarotta, *Sens. Actuators, B*, 2022, **365**, 131906.

212 Y.-J. Yeh, T.-N. Le, W. W.-W. Hsiao, K.-L. Tung, K. K. Ostrikov and W.-H. Chiang, *Anal. Chim. Acta*, 2023, **1239**, 340651.

213 Y. Park, B. Ryu, S. Ki, M. Chen, X. Liang and K. Kurabayashi, *medRxiv*, 2022, preprint, pp. 1–30, DOI: **10.1101/2022.08.01.22278286**.

214 C. M. Das, Y. Guo, G. Yang, L. Kang, G. Xu, H.-P. Ho and K.-T. Yong, *Adv. Theory Simul.*, 2020, **3**, 2000185.

215 E. Zavyalova, O. Ambartsumyan, G. Zhdanov, D. Gribanyov, V. Gushchin, A. Tkachuk, E. Rudakova, M. Nikiforova, N. Kuznetsova and L. Popova, *et al.*, *Nanomaterials*, 2021, **11**, 1394.

216 M. N. Tripathi, K. Singh, U. Yadav, R. R. Srivastava, M. Gangwar, G. Nath, P. S. Saxena and A. Srivastava, *Antiviral Res.*, 2022, **205**, 105382.

217 P. Moitra, M. Alafeef, K. Dighe, M. B. Frieman and D. Pan, *ACS Nano*, 2020, **14**, 7617–7627.

218 Y.-S. Borghei, H. R. Samadikhah and S. Hosseinkhani, *Anal. Chem.*, 2022, **94**, 13616–13622.

219 E. Sobhanie, F. Salehnia, G. Xu, Y. Hamidipanah, S. Arshian, A. Firoozbakhtian, M. Hosseini, M. R. Ganjali and S. Hanif, *TrAC, Trends Anal. Chem.*, 2022, **157**, 116727.

220 Z. Fan, B. Yao, Y. Ding, D. Xu, J. Zhao and K. Zhang, *Chem. Eng. J.*, 2022, **427**, 131686.

221 Z. Zhang, H. Wang, Z. Chen, X. Wang, J. Choo and L. Chen, *Biosens. Bioelectron.*, 2018, **114**, 52–65.

222 E. M. Materón, F. R. Gómez, M. B. Almeida, F. M. Shimizu, A. Wong, K. B. R. Teodoro, F. S. R. Silva, M. J. A. Lima, M. K. S. C. Angelim, M. E. Melendez, N. Porras, P. M. Vieira, D. S. Correa, E. Carrilho, O. N. J. Oliveira, R. B. Azevedo and D. Goncalves, *ACS Appl. Mater. Interfaces*, 2022, **14**, 54527–54538.

223 L. In-Ho, Y. Daehan, A. Phaedon, L. Tony and O. Sang-Hyun, *Nat. Nanotechnol.*, 2019, **14**, 313–319.

224 X. Lin, Z. Liu, T. Stauber, G. Gómez-Santos, F. Gao, H. Chen, B. Zhang and T. Low, *Phys. Rev. Lett.*, 2020, **125**, 077401.

225 W. Yunhao, Z. Yue, B. Audrey, W. Yuru and F. Kin, *Nat. Biotechnol.*, 2021, **39**, 1348–1365.

226 X. Wei, D. Ma, Z. Zhang, L. Y. Wang, J. L. Gray, L. Zhang, T. Zhu, X. Wang, B. J. Lenhart, Y. Yin, Q. Wang and C. Liu, *ACS Sens.*, 2020, **5**, 1707–1716.

227 R. A. Bull, T. N. Adikari, J. M. Ferguson, J. M. Hammond, I. Stevanovski, A. Beukers, Z. Naing, M. Yeang, A. Verich, H. Gamaarachchi, K. W. Kim, F. Luciani, S. Stelzer-Braid, J. S. Eden, W. D. Rawlinson, S. J. van Hal and I. W. Deveson, *Nat. Commun.*, 2020, **11**, 1–8.

228 A. C. Olivieri, N. M. Faber, J. Ferré, R. Boqué, J. H. Kalivas and H. Mark, *Pure Appl. Chem.*, 2006, **78**, 633–661.

229 F. Cui, M. Rhee, A. Singh and A. Tripathi, *Annu. Rev. Biomed. Eng.*, 2015, **17**, 267–286.

230 D. G. Kotsifaki, M. Makropoulou and A. Serafetinides, *J. Nanotechnol. Diagn. Treat.*, 2018, **6**, 1–7.

231 G. A. Lopez, M.-C. Estevez, M. Soler and L. M. Lechuga, *Nanophotonics*, 2017, **6**, 123–136.

232 Q. Liu, H. Yuan, Y. Liu, J. Wang, Z. Jing and W. Peng, *J. Biomed. Opt.*, 2018, **23**, 047003.

233 K. Salimiyan rizi, *Curr. Opin. Electrochem.*, 2022, **32**, 100925.